

## Performance Model of a Recirculating Stack Nickel Hydrogen Cell

Albert H. Zimmerman  
The Aerospace Corporation  
El Segundo, California 90245

A theoretical model of the nickel hydrogen battery cell (Ref. 1) has been utilized to describe the chemical and physical changes during charge and overcharge in a recirculating stack nickel hydrogen cell. In particular, the movement of gas and electrolyte have been examined as a function of the amount of electrolyte put into the cell stack during cell activation, and as a function of flooding in regions of the gas screen in this cell design. Additionally, a two-dimensional variation on this model has been utilized to describe the effects of non-uniform loading in the nickel electrode on the movement of gas and electrolyte within the recirculating stack nickel hydrogen cell. The type of nonuniform loading that has been examined here is that associated with higher than average loading near the surface of the sintered nickel electrode, a condition present to some degree in many nickel electrodes made by electrochemical impregnation methods (Ref. 2). The effects of high surface loading were examined primarily under conditions of overcharge, since the movement of gas and electrolyte in the overcharging condition was typically where the greatest effects of non-uniform loading were found.

The results indicate that significant changes in the capillary forces between cell components occur as the percentage of free volume in the stack filled by electrolyte becomes very high. These changes create large gradients in gas-filled space and oxygen concentrations near the boundary between the separator and the hydrogen electrode when the electrolyte fill is much greater than about 95% of the stack free volume. At lower electrolyte fill levels, these gaseous and electrolyte gradients become less extreme, and shift through the separator towards the nickel electrode. Similarly, flooding of areas in the gas screen cause higher concentrations of oxygen gas to approach the platinum/hydrogen electrode that is opposite the back side of the nickel electrode. These results illustrate the need for appropriate pore size distributions, and the maintenance of both convective electrolyte and gas flow paths through the stack, if the recirculating stack nickel hydrogen cell design is to work properly.

Two models were utilized to examine the role of surface loading. The first of these was like that used in Ref. 3, in which a one-dimensional model allowed a relatively high resolution mapping of cell behavior through the cell stack. The second model was a two-dimensional model that was capable of examining the properties of the cell stack not only across the stack components, but also through the height or width of the individual nickel electrode, separator, or gas screen regions. This second model was applied to cells containing nickel electrodes having surface loading, as well as to cells where the surface loaded nickel electrodes also had surface cracks or localized regions of lower surface loading that could allow a more facile flow of gas or electrolyte. These latter cases allowed the complex interplay of electrode structure, oxygen recombination, and recirculation patterns to be examined in detail, and indicate situations where performance problems specific to a recirculating stack cell could be encountered. The results reported here provide reasonable explanations for many of the popping (i.e. explosive

PRECEDING PAGE BLANK NOT FILMED

hydrogen/oxygen recombination) events observed in nickel hydrogen cells. Furthermore, the results suggest some component and stack design changes that would give this design greater margin to tolerate and properly manage oxygen evolution and recombination without damaging the stack components.

## DESCRIPTION OF MODELS

The basic architecture of the models applied here have been previously described (Ref. 1), and thus will not be discussed in detail here. The general modelling method builds up the desired cell stack design by combining a number of finite elements in the desired physical arrangement. The elements presently available for this purpose include distinct finite elements for the nickel electrode, hydrogen electrode, separator, wall wick, gas screen, and the gas spaces in the cell. The arrangement of these elements indicated in Fig. 1 was used here as the minimum physically reasonable combination of elements for a one-dimensional model of the recirculating stack cell. The configuration of Fig. 1 provides for recombination and stack recirculation by allowing convective and diffusive movement of oxygen gas through the gas screen (elements 4-13), to recombine at the adjoining hydrogen electrode (element 3). The water produced by this recombination can wick into the separator (element 2), the wall wick (element 1), and back into the separator (elements 24-33) between the active nickel electrode (elements 14-23) and the electroactive hydrogen electrode (element 34). This configuration also allows gas and electrolyte flow in response to capillary, convective, and diffusive forces between the nickel electrode, the separator, and the active hydrogen electrode. Elements 35 and 36 provide the gas space that maintains reasonable variation of hydrogen pressure with state of charge in the cell, and also provide convective and diffusive coupling of gas between the cell gas space and the gas screens at the back sides of the platinum electrodes.

The model described by Fig. 1 consisted of 36 elements. To discern the material gradients through the gas screen, separator, and nickel electrode, each of these components was divided into 10 equally sized finite elements. Thus a scan through elements 2-34 provided at any point

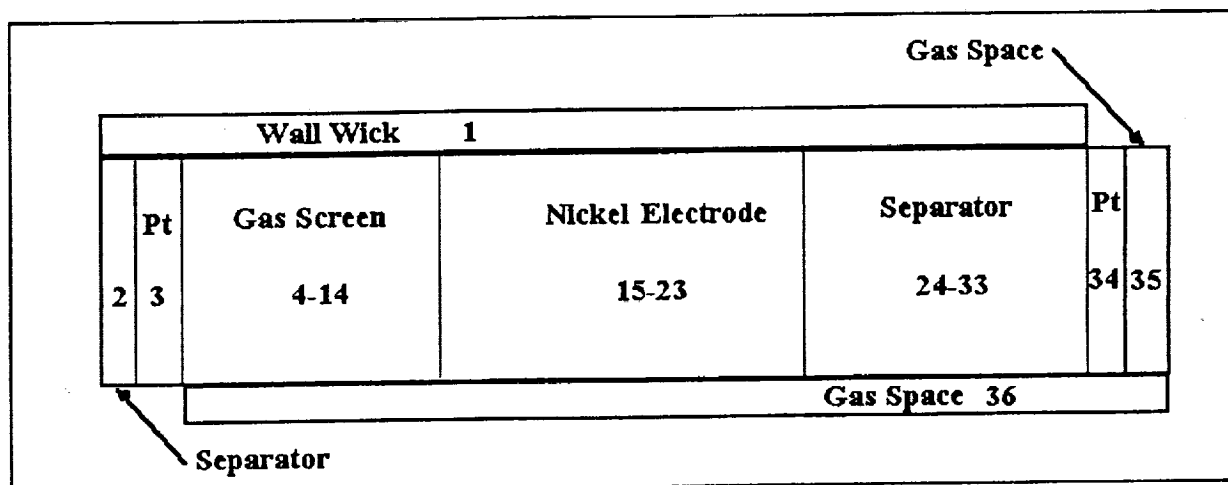


**Figure 1.** Assembly of Finite Elements for Modeling a One-Dimensional Recirculating Stack Nickel Hydrogen Cell.

in time an indication of how element properties (such as oxygen pressure, hydrogen pressure, state-of-charge, electrolyte concentration, or porosity) varied through the repeating stack unit. The component dimensions employed here were a 1 cm<sup>2</sup> area for all components, coupled with thicknesses of 0.3 mm for the separator, 0.16 mm for the hydrogen electrode, 0.5 mm for the gas screen, 0.8 mm for the nickel electrode, and a 0.1 mm thick wall wick. Appendix A lists the data file used in setting up and running the model, and lists all the physical and electrochemical parameters utilized by the model as well as the geometric arrangement of the elements. For the different cells modeled here, the only parameters that were changed were the electrolyte fill in the stack components (hydrogen and nickel electrodes, separator, and wall wick) and the porosity of the gas screen. Thus, the flooding of the gas screen studied herein applies to the situation where approximately 1 cm<sup>2</sup> of the gas screen is partially or fully flooded. Ref. 1 describes the role of each of the parameters listed in Appendix A in considerably more detail.

The cell described in Fig. 1 contains 55 interfaces across which materials such as gas, electrolyte, or solid-state protons can move. Protons were only allowed to diffuse within the active material of the nickel electrode (elements 14-23). Electrolyte was only allowed to move by capillary, convective, or diffusive forces between the stack and wall wick elements (1-3, 14-34). Gas movement was allowed between all elements by either convective or diffusive forces.

The transport of electrons and the charge exchange processes in the cell were modeled using the component arrangement indicated in Fig. 2. Here the microscopic details within the 5-10 micron layers of active material in the nickel electrode described in Ref. 1 have been replaced with a lumped combination of charge transport processes in each nickel electrode element. This provides an excellent characterization of macroscopic performance of the stack, at the cost of poor fidelity for predicting effects due to microscopic depletion in the nickel electrode. For this reason, the voltage of the nickel hydrogen cell at the start of charge, and near the end of discharge is not expected to agree precisely with real cells. The model illustrated in Fig. 2 contains 52 charge transport and charge transfer components, 10 involving nickel electrode sinter conduction, 10 each involving oxygen evolution and  $\beta$ - $\beta$  charge transfer processes, 1 each involving structure conduction and hydrogen oxidation/reduction in the hydrogen electrode, and 20 involving ionic conduction in the electrolyte between elements.

For a more detailed picture of how nickel electrode surface loading could affect cell operation, the two-dimensional model illustrated in Fig. 3 was also used. This 2-D model has the cell components stacked in the x-direction. This model includes a second dimension perpendicular to the stack, in the y-direction. The 2-D model sacrifices some of the spatial resolution in the x-direction to obtain a picture of element parameters in both the x and y-

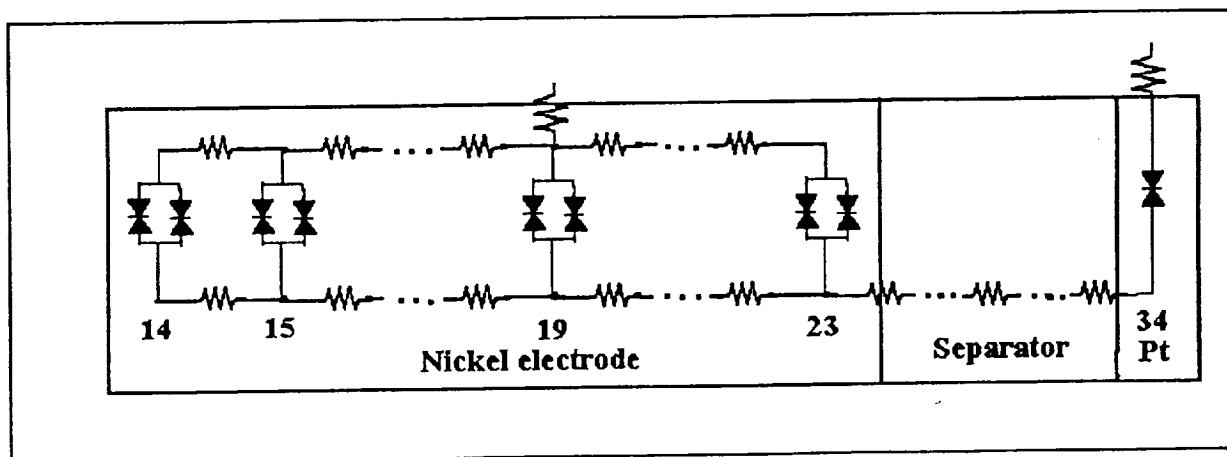


**Figure 2.** Electrical Component Configuration for One-Dimensional Model of a Recirculating Stack Nickel Hydrogen Cell.

directions. In Fig. 3, which includes 45 total finite elements, the element numbers are indicated in each region of the cell. In Fig. 3, each group of three elements in the gas screen, nickel electrode, and the separator are arranged along the x-direction.

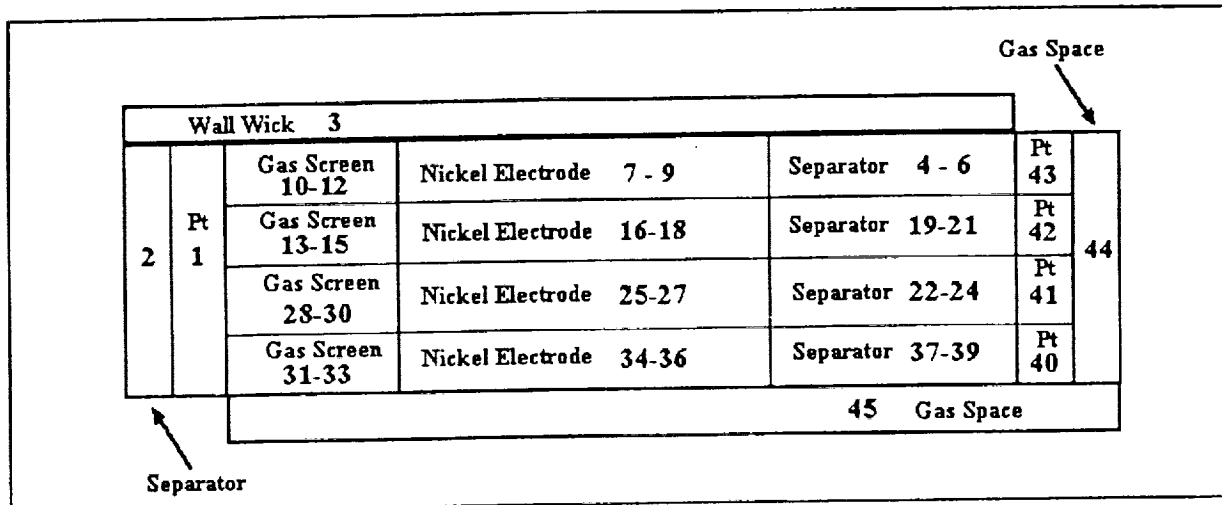


**Figure 3.** Finite Element Assembly for Simulating a Recirculating Stack Nickel Hydrogen Cell in Two-Dimensions.

The physical size of the system modeled here was 1 cm<sup>2</sup> for all stack components in the one dimensional model. For the 2-D model of Fig. 3, the total surface area of the stack components was also 1 cm<sup>2</sup>, however, this area was divided between the different elements in the y-direction according to the details of the system being modeled, as will be discussed later. For example, a crack in the surface of the nickel electrode against the gas screen was simulated by making elements 30-41 0.1 mm high, while elements 4-21, 31-40, and 42-43 were all 3.3 mm high (the crack was actually simulated by giving element 27 a very low loading level). In addition to the 45 finite elements present in the 2-D model, there were 83 interfaces through which gas and/or electrolyte could move, and 95 electrical components describing electronic conduction, ionic conduction, and charge transfer processes. The only charge transfer processes considered here were  $\beta$ -Ni(OH)<sub>2</sub> redox, oxygen evolution, and hydrogen redox processes. The detailed parameters describing these processes and the detailed arrangement of elements, interfaces, and components are given in Appendix B. Ref. 1 describes the role of each of the parameters listed in Appendices A and B in considerably more detail.

Figure 4 indicates the paths for charge transport in the 2-D model, with the 46 electrical nodes being noted. The picture in Fig. 4 can be best thought of as involving a resistive network (highlighted) overlaying a network of ionic conduction, with charge transfer in the nickel and hydrogen electrodes coupling these two networks. The resistive network distributes electrons through the metallic conduction paths of the electrodes, the ionic conduction network describes ionic movement of charge in the electrolyte, with the electrochemical reactions in the nickel and hydrogen electrodes enabling charge conversion between the electronic and ionic charge carriers.

The circles in Figure 4 represent the charge transfer resistances from the Butler-Volmer Eq., with those in the nickel electrode involving the parallel processes of the electrode charge/discharge process and the oxygen evolution process. In the hydrogen electrode, the circles represent the charge transfer resistance of only the hydrogen reaction.

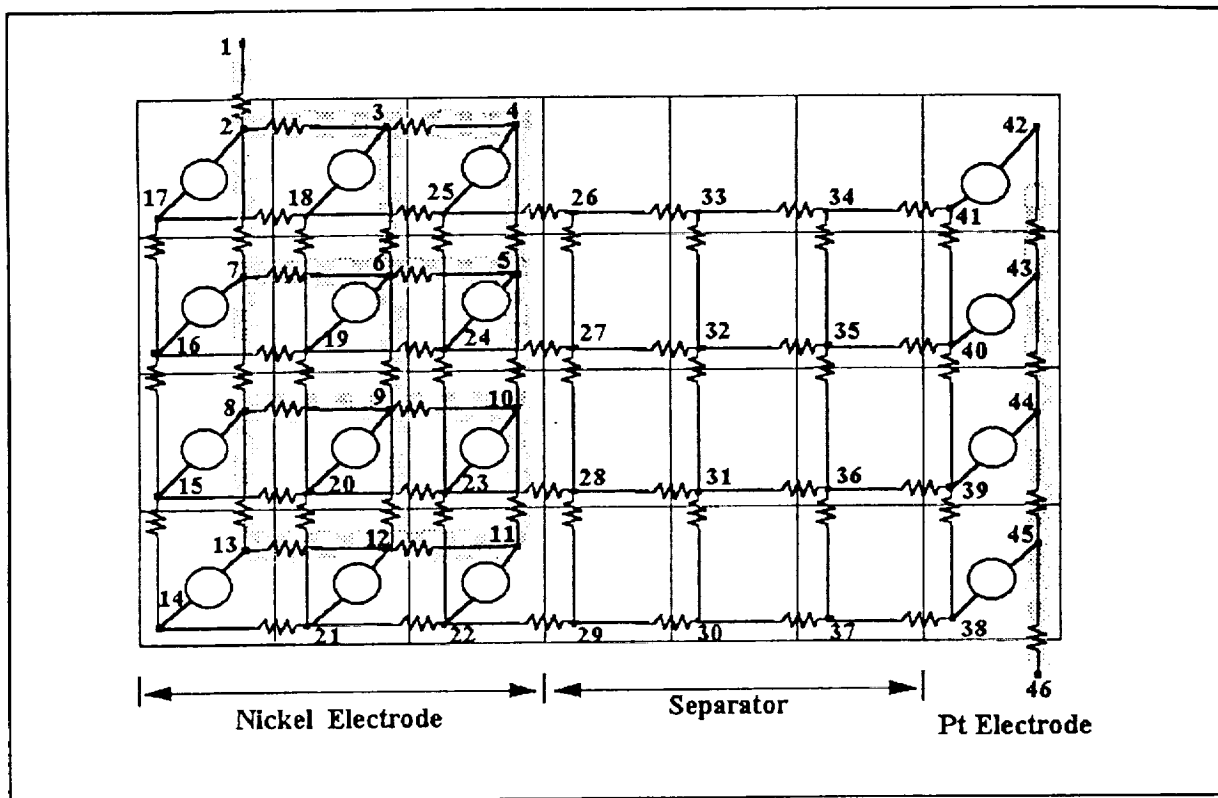


**Figure 4.** Diagram Showing Paths for Charge Transport Through 2-D Model. The Shaded Paths are Electronic Conduction, Circles are Charge Transfer Processes.

## ONE-DIMENSIONAL MODEL RESULTS

### EFFECT OF VARYING ELECTROLYTE FILL IN STACK

The percentage of porosity within the stack of components (excluding the gas screen void volume) was varied from 88% to 99%, with the latter fill being very close to a flooded cell. The model was then used to determine where the electrolyte ends up and where gases flow during charge at  $2 \text{ ma/cm}_2$  (about  $C/10$ ) for 80,000 sec, which is long enough to bring the cell into oxygen evolution at about 90% of the applied current (i.e. 10% charge efficiency). Figure 5 indicates the typical cell voltage and pressure profiles during charge. Voltage and pressure did not change much as the amount of electrolyte in the stack was varied at these relatively high levels. The lack of a clear transition into overcharge is because the temperature was 20 deg C. At lower temperatures there appears a much clearer distinction between recharge and overcharge, as the oxygen evolution potential increases relative to the recharge potential.

The cell charge was started from an initial state where 0.01 atm of oxygen was artificially present in the gas space, and 2.0 atm of hydrogen gas was initially present in the discharged cell. In some of the data that follows, effects are seen early in the recharge from recombination of this oxygen. After this early equilibration period, the oxygen pressure in the cell was generally low early in the charge period, rising to much higher values at the end of charge. Figures 6 and 7 indicate the variation in oxygen pressure across the stack at 10,000 sec, when the cell is not in

overcharge, and at 80,000 sec, when the cell is in overcharge. These figures clearly show the profile of higher levels of oxygen in the nickel electrode, since this is where the oxygen is being generated. They also show higher levels of oxygen moving into the separator from the nickel electrode as the amount of electrolyte in the stack is increased. At very high levels of electrolyte, this can result in a very steep gradient in oxygen pressure near the surface of the platinum electrode. This is a situation in which it is very possible to form actual bubbles of oxygen gas. It should be noted that this model does not differentiate between gas bubbles and uniformly dispersed gas.

Figure 8 indicates the change in oxygen pressure with time during charge in element 20, which is in the center of the nickel electrode. The oxygen pressure is at its maximum level in this element, since the source of the oxygen is the nickel electrode. Figure 8 shows how the oxygen pressure starts to build up, particularly at the center of the nickel electrode as the cell goes into overcharge at about 36,000 sec. A very similar time dependence for the buildup of oxygen was observed in the other elements of the cell, however because transport of oxygen to the Pt catalyst electrodes was more facile than from element 20, the pressures attained during overcharge were less than in element 20.

Figures 9 and 10 indicate the variation in porosity through the cell stack at 10,000 sec into charge (when very little oxygen evolution occurs), and at 80,000 sec (when most of the charge current is going into oxygen evolution. The porosity, as defined here, refers to the fraction of the element volume available to contain gas, thus is not filled with solid materials or electrolyte. As shown in Fig. 9, when little oxygen is being evolved, there is a large porosity gradient between the hydrophobic Pt catalyst electrode and the separator and nickel electrodes. This is particularly true at high KOH fill levels where both the separator and the nickel electrode are nearly flooded with electrolyte. When there is significant oxygen evolution and recombination (Fig. 10), while the Pt electrode porosity is not changed much, the separator porosity is increased significantly by the movement of oxygen through the separation region. In full overcharge (2 ma/cm<sup>2</sup>) at 80,000 sec, most of the oxygen is transported through the gas screen to recombine on the back side of the adjacent Pt electrode. However, at electrolyte fill levels less than 90%, a very significant fraction of the generated oxygen diffuses as gas through the open spaces in the separator material to recombine on the Pt catalyst.

The development of the porosity during the 80,000 sec charge period is indicated in Figs. 11-13, for elements 15, 24, and 34, respectively. In element 15 (nickel electrode) the porosity generally increases through the charge period as the flux of oxygen migrating through the nickel electrode in this region to the gas screen increases. In element 24 (separator), the porosity at high electrolyte fill levels does not change much with oxygen evolution since there is little space for electrolyte to move into. This behavior illustrates that capillary forces essentially disappear at high electrolyte fill levels, since essentially all pores are filled with electrolyte. Most of the free volume tends to end up in the hydrophobic regions of the Pt catalyst electrode. Interestingly, in Fig. 12 with a 98% fill factor or less, a significant upswing in porosity is seen in the separator commencing when oxygen evolution begins, essentially a result of the interplay of increasing capillary forces and the pressure of oxygen evolution and movement from the nickel electrode towards the Pt catalyst. Element 34 (Fig. 13, Pt electrode) indicates that there is a threshold of electrolyte fill at about 95-96%, such that if more electrolyte is present some flooding of the Pt electrode occurs as the Pt electrode recombines oxygen, largely because the other cell components are not able at these high fill levels to wick the electrolyte from the Pt electrode. As the charging continues and gas pressure builds up, more space becomes available in the cell (active

material density increases), and the porosity of the Pt electrode increases. At electrolyte fill levels below 95%, the higher porosity in the Pt electrode is always maintained, because the other cell components are capable of effectively wicking electrolyte at all times.

The concentration of electrolyte varies across the stack in a dynamic way dictated by all reactions in the cell. Fig. 14 indicates the concentration gradient at 10,000 sec into charge, when essentially no oxygen is being evolved. The concentration of KOH is lower in the nickel electrode because water is being generated by the charging reaction, and is higher in the platinum electrode (element 34) because water is being consumed in the generation of hydrogen. These processes maintain about a 2% concentration gradient across the stack modeled here, with little changes being seen in the KOH concentration at the recombination Pt electrode or the wall wick.

However, when oxygen is being evolved (Fig. 15, 80,000 sec into charge) a significant reduction in the KOH concentration in the recombination Pt electrode is seen due to the recombination of oxygen that passes through the gas screen. It should be noted here that this quite low KOH concentration would actually be dispersed across a more extended stack of plate components in a real cell, since an electroactive Pt electrode would cancel out much of the lowered concentration seen here in element 2. The variation in KOH concentration in element 2 also shows that at KOH fill factors above 90-95% the ability of the wall wick to effectively transport electrolyte falls off dramatically. In the remainder of the stack the loss of oxygen to the recirculation process results in a slightly increased concentration profile, all the while maintaining the approximately 2% gradient between the Ni and Pt plates.

Figs. 16-19 focus on the changes in KOH concentration during the full 80,000 sec charge period in elements 2, 15, 24, and 34 respectively. These elements represent the recombination Pt electrode, the nickel electrode, the separator, and the Pt/H<sub>2</sub> electrode. These figures show the KOH concentration dropping in the recombination Pt electrode (element 2) when significant oxygen evolution begins, and at the same time a significant increase in the remainder of the stack (elements 15-34).

It is typically assumed that the nickel electrode charges and discharges uniformly through the thickness of the sintered electrode, simply because the sinter structure is both highly porous and highly conductive. Figures 20 and 21 indicate the gradient in state-of-charge realized across the nickel electrode at 10,000 and 80,000 sec into a 2 ma/cm<sup>2</sup> charge. In Fig. 20 it is clear that the nickel electrode charges more efficiently on the side facing the separator and the Pt/H<sub>2</sub> electrode. This is primarily because of the ionic resistance in the electrolyte through the nickel electrode, with some contribution from the varying oxygen activity and KOH concentration through the nickel electrode. In Fig. 21, this state-of-charge variation through the thickness of the sinter is reduced as the electrode approaches the fully charged state. Fig 21 also shows a cumulative effect of electrolyte fill level on charge efficiency. High fill factors give improved charge efficiency. A number of factors contribute to this effect. First, the greater amount of electrolyte reduces the ionic resistance. Second, the higher oxygen pressure in the nickel electrode slightly improves the charge efficiency by reducing the oxygen evolution rate. Finally, the slightly elevated KOH concentration associated with the higher electrolyte fill factors act to slightly improve charge efficiency.

## EFFECTS OF GAS SCREEN FLOODING

The effect of flooding the gas screen in a region of the nickel hydrogen is of interest, because some cell activation procedures may leave excess amounts of electrolyte trapped in the gas screen. Intuitively, it seems clear that this will limit gas transport in and out of the hydrogen electrode, and if enough of the gas screen is flooded, severe impacts on the cell performance will result. The gas screen flooding modeled here was done assuming that only 1 cm<sup>2</sup> of the gas screen is flooded. This is insufficient to significantly affect the electrical performance of the cell much, since there is very little overpotential associated with the hydrogen electrode. However, gas screen flooding will redirect oxygen transport in the flooded regions, giving local areas of higher than normal oxygen pressure. This was modeled here by filling the gas screen region of elements 4-13 with KOH in a 1 cm<sup>2</sup> area. The model was then run with several electrolyte fill levels: 95 and 98%.

Figure 22 indicates the variation in oxygen pressure through the stack when the gas screen is flooded, in comparison with a non-flooded gas screen. Clearly, the flooded gas screen allows high pressures of oxygen gas to approach the Pt electrode through the gas screen. In addition, the increased oxygen flux forced through the nickel electrode and the separator results in considerably higher oxygen pressures through the separator and approaching the active Pt/H<sub>2</sub> electrode. Clearly this situation significantly increases the likelihood of popping, i.e. explosive recombination of oxygen on the Pt surface when the oxygen concentration locally exceeds 4% of the hydrogen (about 1 atm oxygen here).

Figure 23 indicates how gas screen flooding affects the porosity of the cell stack when the cell is in overcharge. The flooding of the gas screen has little effect by itself on the porosity of the components, since this is primarily dictated by the amount of electrolyte in the stack coupled with the pore size distributions of the components. If this model were run in a mode where the electrolyte was not trapped in the gas screen, but could undergo free transport in or out of the stack, greater effects would be seen on the porosity in the stack components.

Figure 24 indicates how gas screen flooding affects the electrolyte concentration gradient through the stack when the cell is in steady-state overcharge (i.e. at 80,000 sec into charge). Again, while gas screen flooding reduces the electrolyte concentration throughout the stack by about 0.3%, there is little change in this concentration profiles for cells of differing KOH fill levels which have flooded gas screens. There is a significant interplay between the KOH fill and gas screen flooding in terms of the wall wick function in the cell. This is because the wall wick loses its capillary function above 95-96% KOH fill, in addition to the change in oxygen recombination as the gas screen floods. Thus, in Fig. 24, at a 95% KOH fill, a cell with a flooded gas screen will tend to wick some electrolyte from the stack, while this essentially is turned off at a 98% KOH fill.

A significant driving force for degradation in nickel hydrogen cells during overcharge, and for developing oxygen bubbles and popping, is the pressure differential developed across the stack components as the cell is charged and discharged. In overcharge it is possible to build up a significant overpressure of oxygen gas if the gas transport is sufficiently inhibited by low component porosity, or the gas evolution rate is sufficiently high. Fig. 25 indicates the pressure differential resulting from the model runs described above at the 80,000 sec point in charge, i.e. when the cell is in overcharge. Fig. 25 plots the maximum pressure differential between the nickel electrode and the separator or gas screen elements adjacent to the Pt electrodes. With the normally functioning gas screen, very little pressure differential is seen until the KOH fill reaches

96-98%. When areas of the gas screen become flooded, the pressure differential is increased 4-5 times. With a flooded gas screen region, electrolyte fill levels above about 90% will likely result in a significant pressure differential across the stack. Clearly, the location of electrolyte in the cell can play a large factor in establishing stress levels during overcharge, and cumulative stress during long term cycling.

## RESULTS WITH NON-UNIFORM LOADING

Four differing non-uniform loading profiles in the nickel electrode were examined in comparison with a uniform loading of 1.6 g/cc void. Figure 26 indicates these four loading profiles. Profile A has high loading only on the gas screen side of the nickel electrode. Profile B has high loading only on the separator side, while profiles C and D have high and moderate loading on both surfaces of the nickel electrode. As indicated in Fig. 26, the loading drops linearly to a minimum level in the center of the nickel electrode. The total amount of active material in the nickel electrode is maintained at a constant level in all these simulations. All of these simulations started with 95% of the volume in the components being filled with 31% KOH electrolyte. Other pertinent parameters are indicated in Appendix B. The simulations that were run consisted of charging at 2 ma/cm<sup>2</sup> for 80,000 sec, long enough to charge the cell and to be in overcharge. Typically, the cell was 92% charged by this charge cycle, and the internal hydrogen pressure was 27-28 atm, depending on the quantity of oxygen in the cell when it was in overcharge. The pore size distribution in the nickel electrode was assumed to shift linearly from a generic distribution measured for a relatively uniformly loaded electrode, towards smaller pore sizes according to the remaining free volume in the nickel electrode elements. A density of 3.6 g/cc was used for the nickel electrode active material, thus it was not possible to fill the pores with active material beyond this density.

Figure 27 indicates the effect of non-uniform loading on the buildup of oxygen in the cell components during the charge, showing oxygen partial pressure at the end of the recharge period. The oxygen builds up in the nickel electrode as the cell goes into overcharge, being quite low prior to overcharge. The high surface loading prevents the diffusion of oxygen from the nickel electrode, thus resulting in very high partial pressures of oxygen. Figure 27 indicates the oxygen partial pressure through the stack for loading profiles A-D in Fig. 26, along with the uniformly loaded case. In the case where the high surface loading exists on both surfaces of the nickel electrode, the total pressure in the nickel electrode exceeds that outside the nickel electrode, since even the strong convective flows in the stack are unable to move enough through the nickel electrode surfaces to maintain uniform pressure. This is shown in Fig. 28. These pressure differentials clearly can exert significant stress on the structure of the nickel electrode, possibly contributing to swelling, active material being forced from the pores and into the separator, and blistering.

Fig. 29 compares the electrolyte concentrations for uniformly and non-uniformly loaded nickel electrodes when in overcharge. Local concentration gradients clearly become much more significant when the nickel electrode has local areas of high loading, particularly when the highest loaded areas are adjacent to the separator rather than near the gas screen. These localized areas of high loading tend to support most of the oxygen evolution and charging reactions, thus developing a more strongly graded electrolyte concentration.

## TWO-DIMENSIONAL MODEL RESULTS

The two dimensional model described earlier was first run with a uniform loading level in the nickel electrode of 1.6 g/cc void. The results from this simulation are indicated in Figure 30, which shows the percentage of oxygen in the gas phase present within the cell as a function of position within each component. The slightly increased oxygen levels at the top of the cell result from electrolyte recirculation through the wall wick from the Pt electrode on the left, to the separator on the right. This pumps some additional electrolyte into the top of the separator on the right side of the stack in Fig. 30, thus slightly inhibiting oxygen diffusion in this wetter region. As indicated by Fig. 30, the oxygen level only reaches a 4-5% concentration in the middle of the nickel electrode, with levels under 1% existing in the separators and gas screens. Clearly in this case there is facile transport of gas and liquid components through the cell, and there is little risk of popping or other phenomena associated with the buildup of oxygen in the stack. Figure 30 indicates the way the nickel hydrogen cell is supposed to work in terms of gas and electrolyte transport.

Another simulation was run with surface layers 25% of the thickness of the nickel electrode on each side of the electrode. These surface layers were loaded at 3.1 g/cc void. The inner 50% of the electrode thickness was loaded at a level which gave an average loading level of 1.6 g/cc void. It should be noted here that the cell voltage during recharge differed by less than 5 mv between the surface loaded cases and the uniformly loaded cases, with the voltage being slightly higher when the loading was not uniform. Figure 31 indicates contours of oxygen concentration for this case. The oxygen level in the nickel electrode is dramatically increased, with oxygen levels over 80% being obtained in the center of the nickel electrode near the bottom of the stack. Oxygen concentrations as high as 2% penetrate as far as 50% of the way through the separator towards the Pt electrode. Although these oxygen levels are quite high, they are dissipated in a relatively uniform way through the separator and gas screen such that the Pt electrode is not exposed to oxygen concentrations over 1%. This is well below the level of 4% required to initiate a popping event, i.e. a localized hydrogen/oxygen explosion.

The asymmetry between the top and the bottom of the stack in Fig. 31 is again due to the recirculation of electrolyte through the wall wick at the top of the cell. This characteristic recirculation pattern gives higher oxygen levels at the top of the cell. The increased oxygen level at the bottom of the nickel electrode and the adjacent separator is likely to result from gas transport being more facile away from the boundaries of the cell.

Variation in the transport of gas in the y-direction in the cell was modeled by putting a small crack in the position of element 27, which was on the side of the nickel electrode against the gas screen. This crack was a surface region 0.1 mm high and 25% of the electrode thickness, and which was loaded at 0.115 g/cc void. The remaining regions of the nickel electrode were loaded at 0.115 g/ccv if in the center, and 3.1 g/ccv if on the surface. Thus, element 27 provided a channel for gas flow out of the nickel electrode. Clearly, if surface loading exists in nickel electrodes, there will be areas having lower loading and other areas where actual channels exist to allow gas flow out of the electrode. The crack designed into the electrode is meant to simulate these kinds of areas.

Figure 32 indicates the results of this simulation in the form of contours of oxygen concentration throughout the cell stack. As expected, the oxygen preferentially moves out of the nickel electrode and into the gas screen through the crack, giving a small region in the gas screen where a higher concentration of oxygen exists. Because the gas screen allows facile movement

and diffusion of gas, high concentrations of oxygen do not penetrate very far into the gas screen region. Thus, as long as the gas screen is maintained relatively free of entrapped electrolyte, there appears to be little risk of igniting the high oxygen levels in the nickel electrode through the gas screen. Interestingly, a secondary effect of the crack in the nickel electrode in Fig. 32 is that it forces a stronger recirculation pattern by channeling the oxygen through the gas screen. This recirculation pattern is recognized by the curvature of the oxygen contours at the top of the cell stack in Fig. 32. However, the oxygen gradients are still greatest at the surface of the nickel electrode, and oxygen concentrations up to 4% still only penetrate about 50% of the way through the separator.

A final simulation, which was very similar to that of Fig. 32, was done, except that the crack was put on the separator side of the nickel electrode (in the element 25 position). The size and loading associated with this crack were the same as previously described. Fig. 33 shows the contours of oxygen in the cell stack obtained during overcharge. The increased oxygen transport through the crack is seen as a bulge in the contours in the separator on the right side of the cell. As it propagates through the separator, this bulge moves upward, until about 75% of the way to the top of the stack, it touches the Pt electrode at an oxygen concentration of about 4%. It is clearly possible in this situation to ignite the oxygen, and potentially to propagate an ignition front back toward the nickel electrode. Interestingly, if the bulge were to propagate uniformly across the separator, it is unlikely that it would reach the Pt electrode at a 4% oxygen level. The recirculation of electrolyte into the top of the separator makes the dissipation of the oxygen bulge much more difficult near the top of the stack. In addition, some oxygen is being channeled through the wall wick and into the separator on the left side of the stack. These effects from the recirculation process accentuate the increased oxygen concentration in the separator in regions where the wall wick contacts separator. The increased wetness of the top of the separator on the right side of the stack also results in a significantly higher concentration of oxygen within the top of the nickel electrode, where much of the internal volume contains more than 80% oxygen gas.

Clearly, the variation of separator wetness possible in a recirculating design can increase the likelihood of popping if surface loading exists, particularly when compared to a back-to-back design where oxygen is expected to move much more uniformly across the separator. Note that the bottom of the separator on the right side, which is the driest region, is carrying the majority of the oxygen gas, but the 4% oxygen contour reaches only a little more than 50% of the way through the separator.

## CONCLUSIONS

The behavior described above for a recirculating stack nickel hydrogen cell is in all cases exactly what would be expected based on the present qualitative physical understanding of the nickel hydrogen cell. The results of this model, however, allow the details of cell performance and operation to be better quantified, and provide some visibility into how the various physical and electrochemical processes operate at a microscopic scale through the component stack. This information can serve as a useful guide for those who design and operate nickel hydrogen cells.

The results of the studies reported here indicate that the transport of gas and electrolyte through the nickel hydrogen cell can have very significant effects on the performance of the cell, depending on the amount and location of electrolyte in the cell. For the recirculating stack

design modeled here, as well as for other cell designs, it is necessary to maintain appropriately designed gas and electrolyte management processes during all periods of cell operation. In the recirculating stack modeled here, it is clear that if the fraction of stack void volume filled with electrolyte exceeds a threshold of 90-95%, significant changes in the internal cell operation occur. Capillary forces become exceedingly weak, wall wicks become much less effective, and the interface between the separator and the Pt electrode can become the site of large gradients in porosity and oxygen pressure.

If the gas screen in the recirculating stack is allowed to flood in localized regions, high oxygen pressures are allowed to approach the Pt electrode through the gas screen. Clearly these results have ramifications both in terms of how the nickel hydrogen cell stack is designed, how individual components are manufactured, and how cells are activated with electrolyte. Further modeling of specific activation processes could be most instructive in indicating techniques to prevent popping and to assure appropriate electrolyte fill levels in the cell. These results clearly show that the major material conversion and transport processes in the nickel hydrogen cell can be usefully modeled, and that the results can provide guidance to cell designers, manufacturers, and users.

The effects of non-uniform nickel electrode loading on the operation of a recirculating stack nickel hydrogen cell were modeled, and it was found that variations in loading levels within the nickel electrode can have a profound effect on local levels of oxygen in the cell, and can also affect local electrolyte concentrations during recharge, and presumably discharge. Loading variations can channel oxygen generated from overcharging the nickel electrode either into the gas screen, or into the separator. Channeling such oxygen into a relatively dry gas screen was found to have no undesirable consequences for a C/10 overcharge rate. Channeling oxygen into the separator was found to couple into the recirculation pattern in the cell such that oxygen concentrations in excess of 4% could contact the Pt electrode. Such contact occurred in regions where separator wetness was maximized by the recirculation process. The coincidence of an area of high wetness due to the cell recirculation path with an area on the nickel electrode surface that channels oxygen into the separator, could lead to very serious popping within the nickel hydrogen cell.

## REFERENCES

1. A. H. Zimmerman, *Proc. 183rd Meeting of the Electrochemical Society, Vol. 93-1, The Electrochemical Soc. Inc., Pennington, N. J., 1993, p. 147.*
2. A. H. Zimmerman, *Performance Model of a Nickel Hydrogen Cell, The Aerospace Corporation, to be published.*
3. A. H. Zimmerman, *Performance Model of a Recirculating Stack Nickel Hydrogen Cell, The Aerospace Corporation, to be published.*

## ACKNOWLEDGEMENT

This work was supported by the Aerospace Corporation, as part of the ASR Program, and by NASA, Lewis Research Center. Support from both these sources is gratefully acknowledged.

Fig. 5. Recirculating Stack NiH<sub>2</sub> Cell  
Charge at 2 ma/cm<sup>2</sup> from 0.01 SOC, 20 C

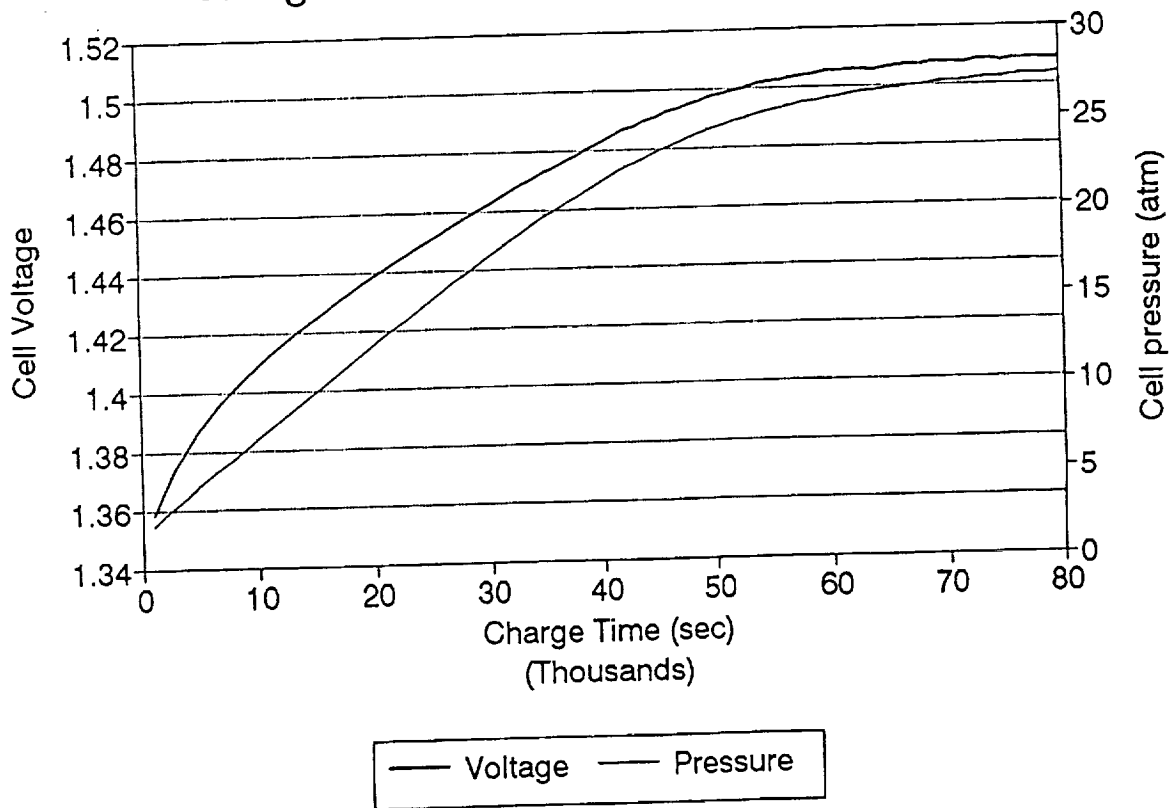


Fig. 6. Recirculating Stack NiH<sub>2</sub> Cell  
Oxygen Pressure at 10Ks into Charge

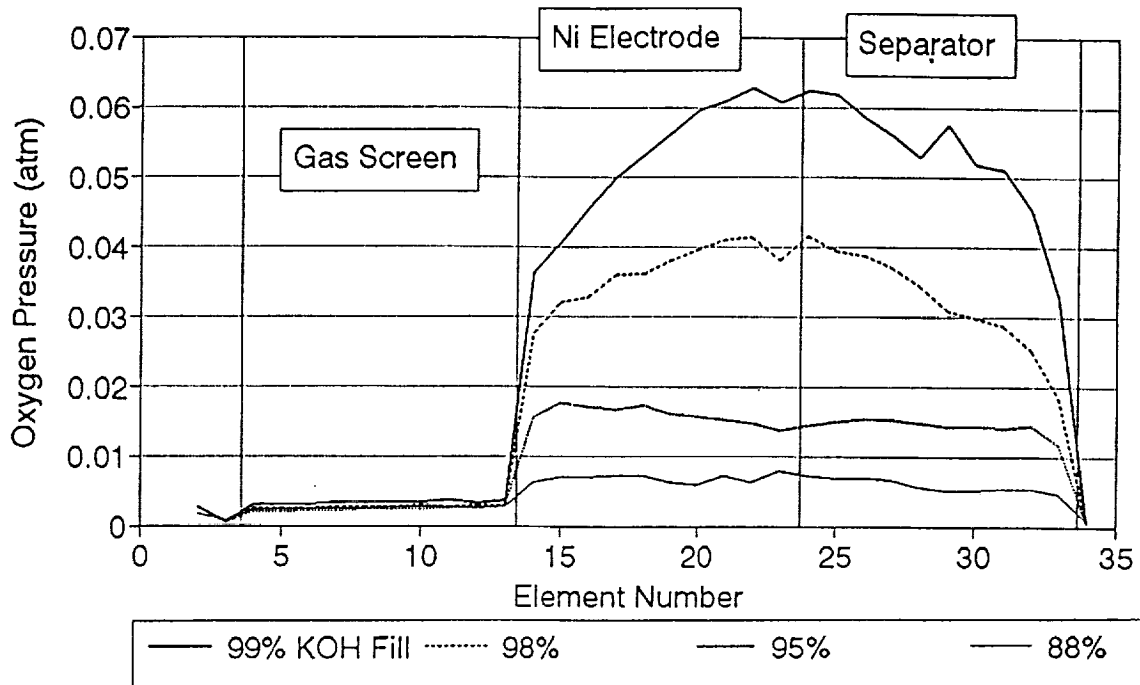


Fig. 7. Recirculating Stack NiH<sub>2</sub> Cell  
Oxygen Pressure at 80Ks into Charge

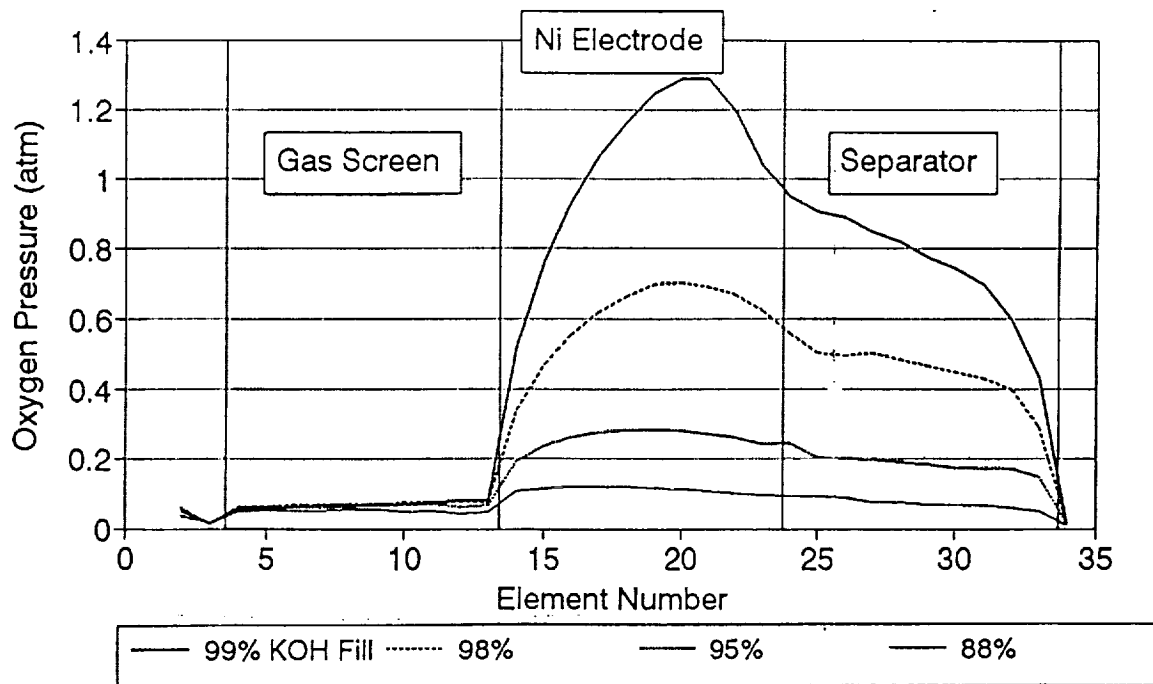


Fig. 8. Recirculating Stack NiH<sub>2</sub> Cell  
Oxygen Pressure During Charge, Elem 20

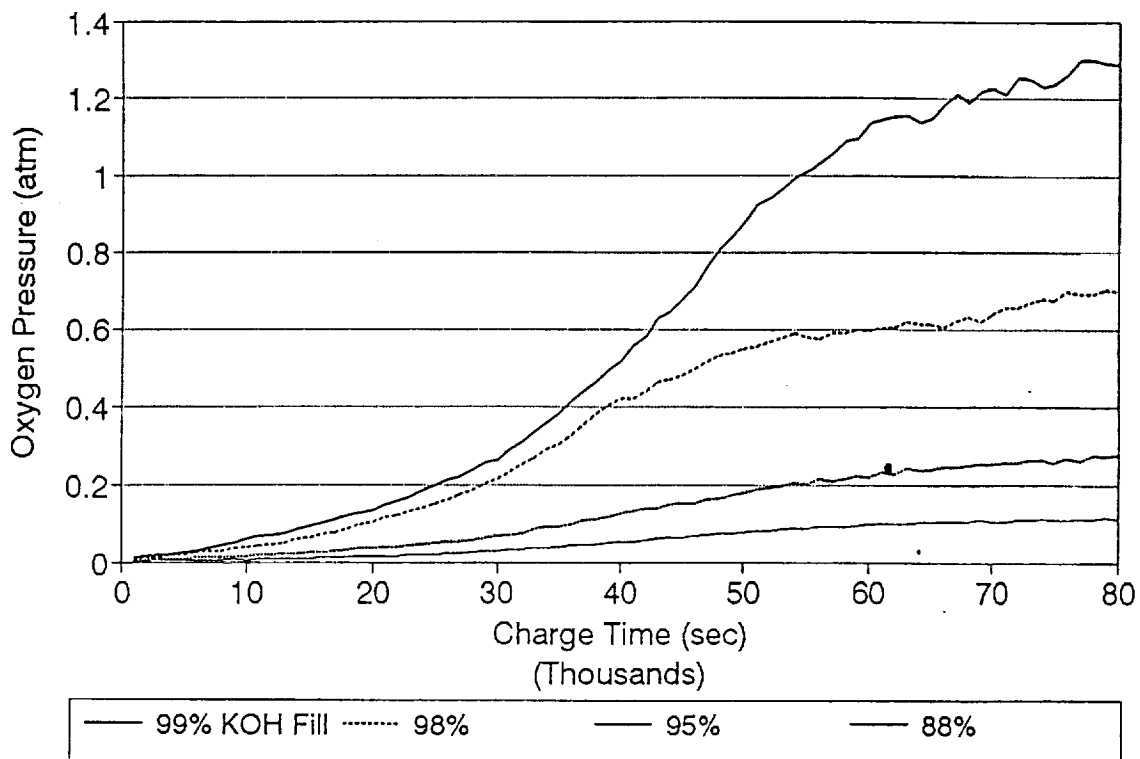


Fig. 9. Recirculating Stack NiH<sub>2</sub> Cell  
Stack Porosity at 10Ks into Charge

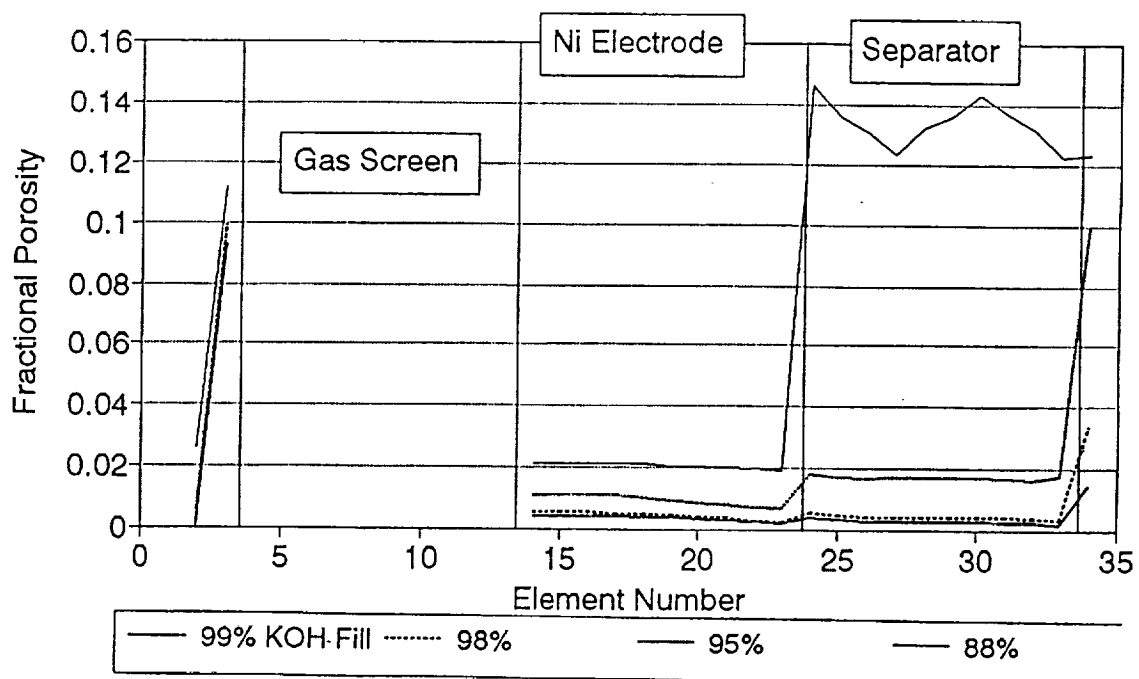


Fig.10. Recirculating Stack NiH2 Cell  
Stack Porosity at 80Ks into Charge

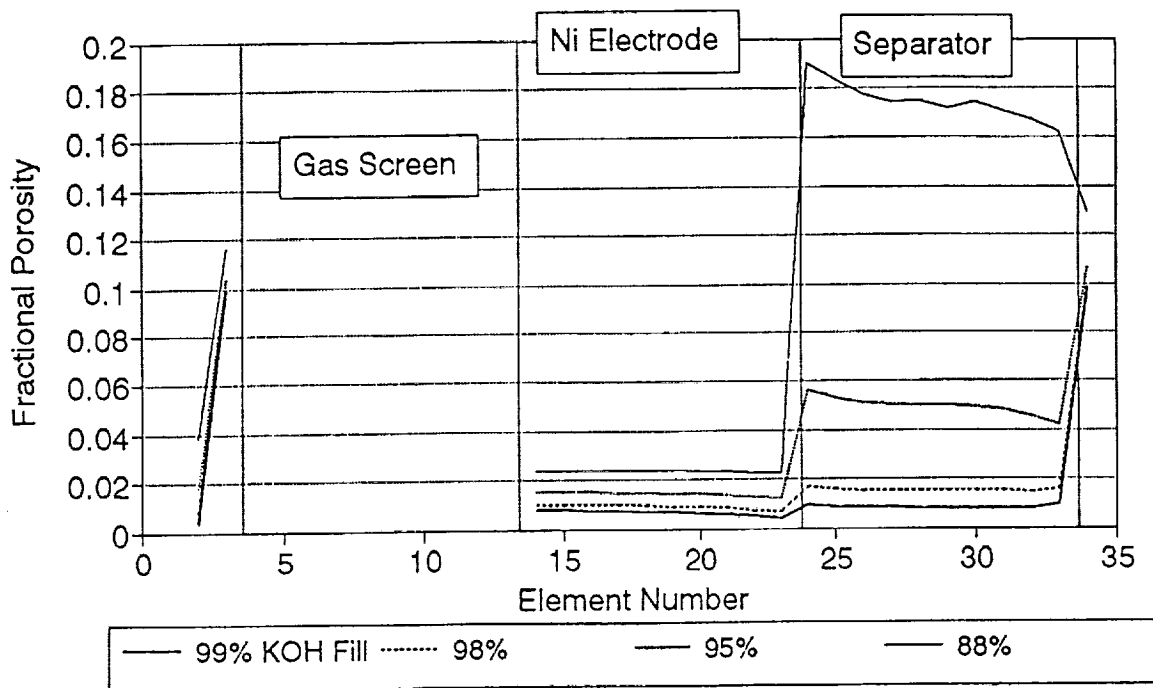


Fig. 11. Recirculating Stack NiH2 Cell  
Porosity During Charge, Ni Elem 15

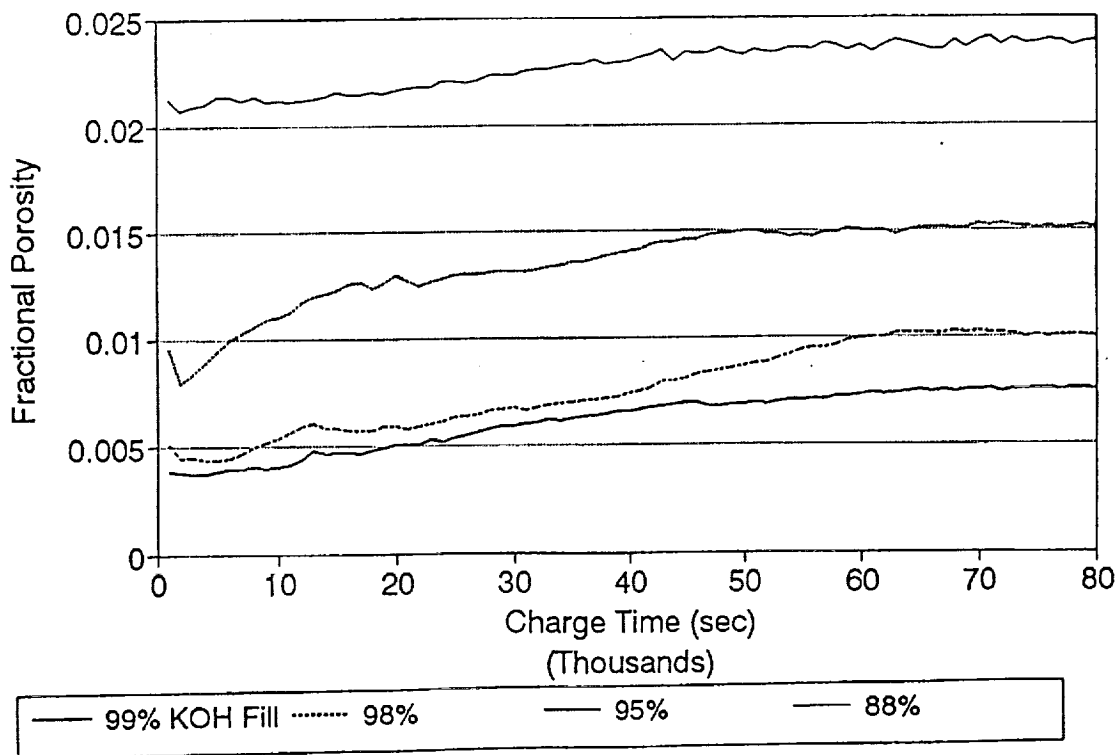


Fig. 12. Recirculating Stack NiH2 Cell  
Porosity During Charge, Sep Elem 24

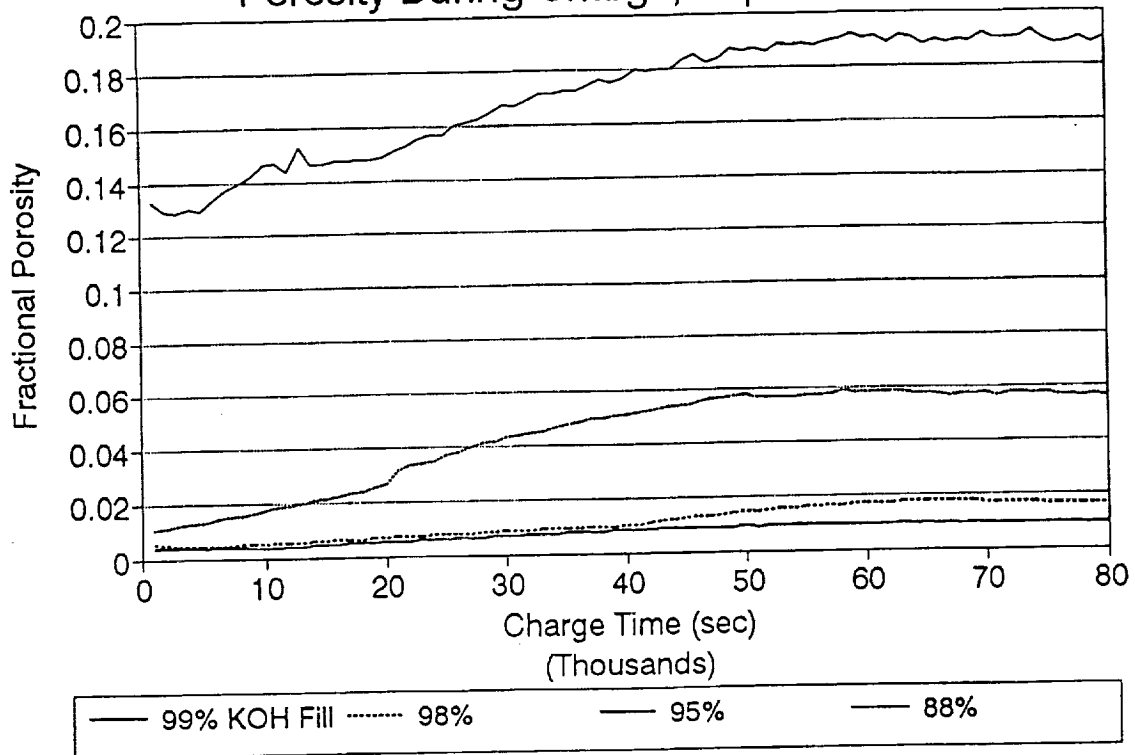


Fig. 13. Recirculating Stack NiH2 Cell  
Porosity During Charge, Pt/H2 Elem 34

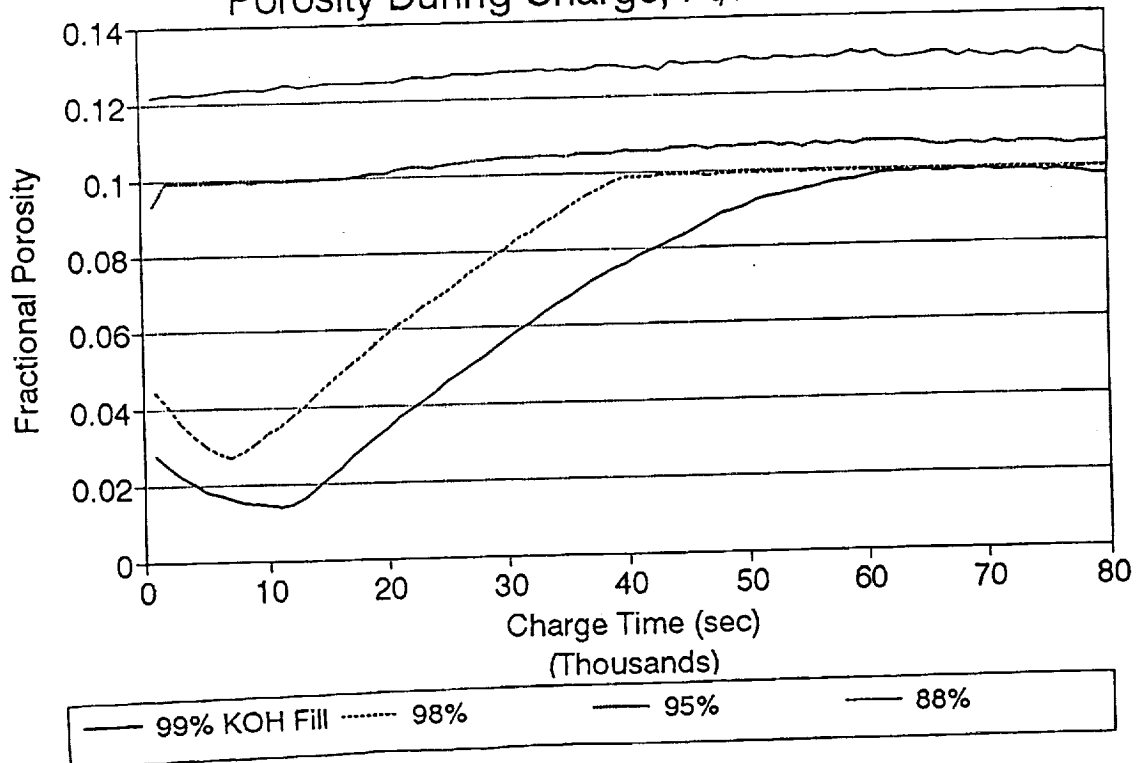


Fig. 14. Recirculating Stack NiH<sub>2</sub> Cell  
% KOH Concentration at 10Ks into Charge

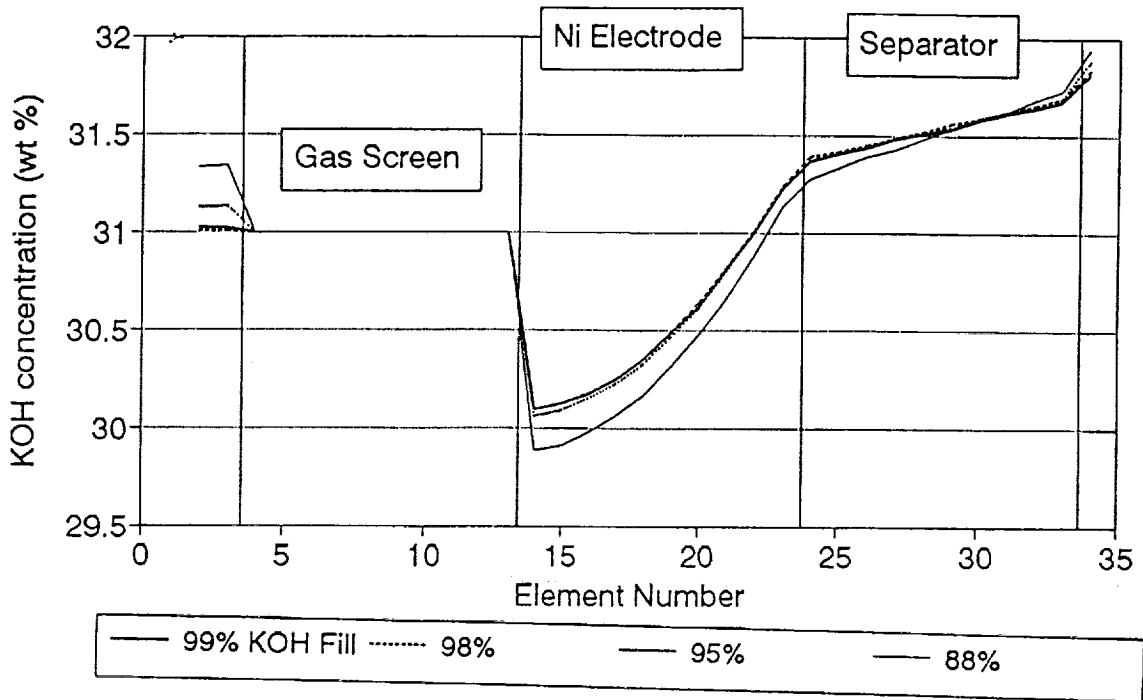


Fig. 15. Recirculating Stack NiH<sub>2</sub> Cell  
% KOH Concentration at 80Ks into Charge

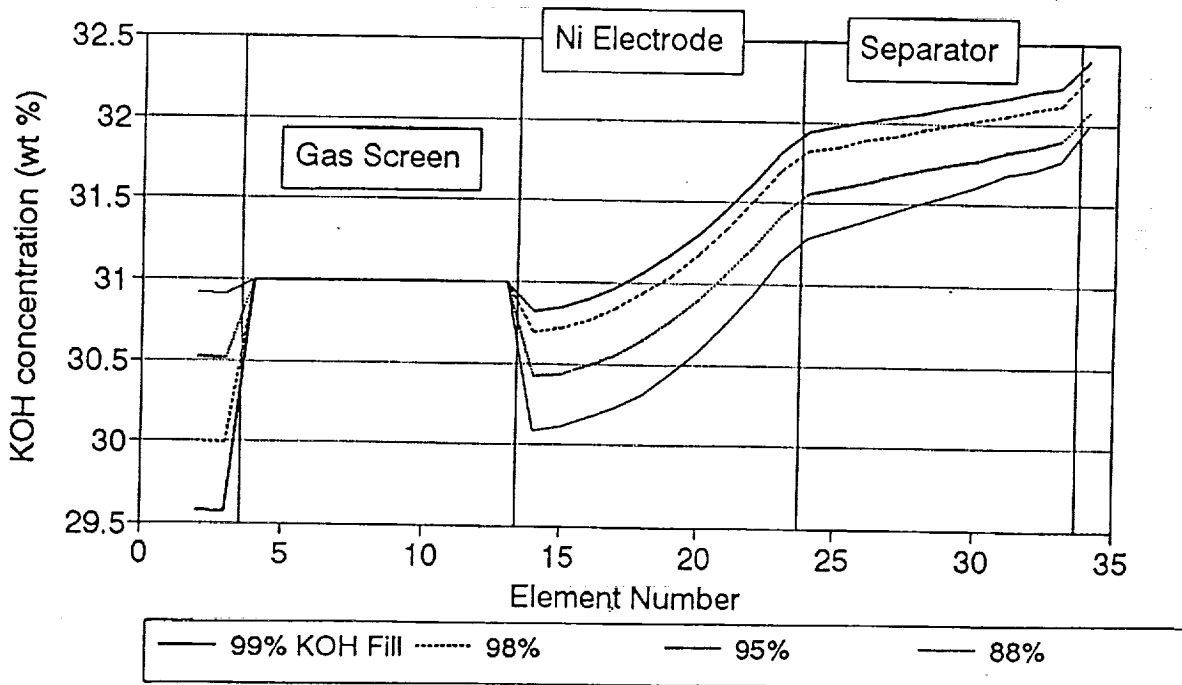


Fig. 16. Recirculating Stack NiH2 Cell  
 Conc KOH During Charge, Recom Sep Elem 2

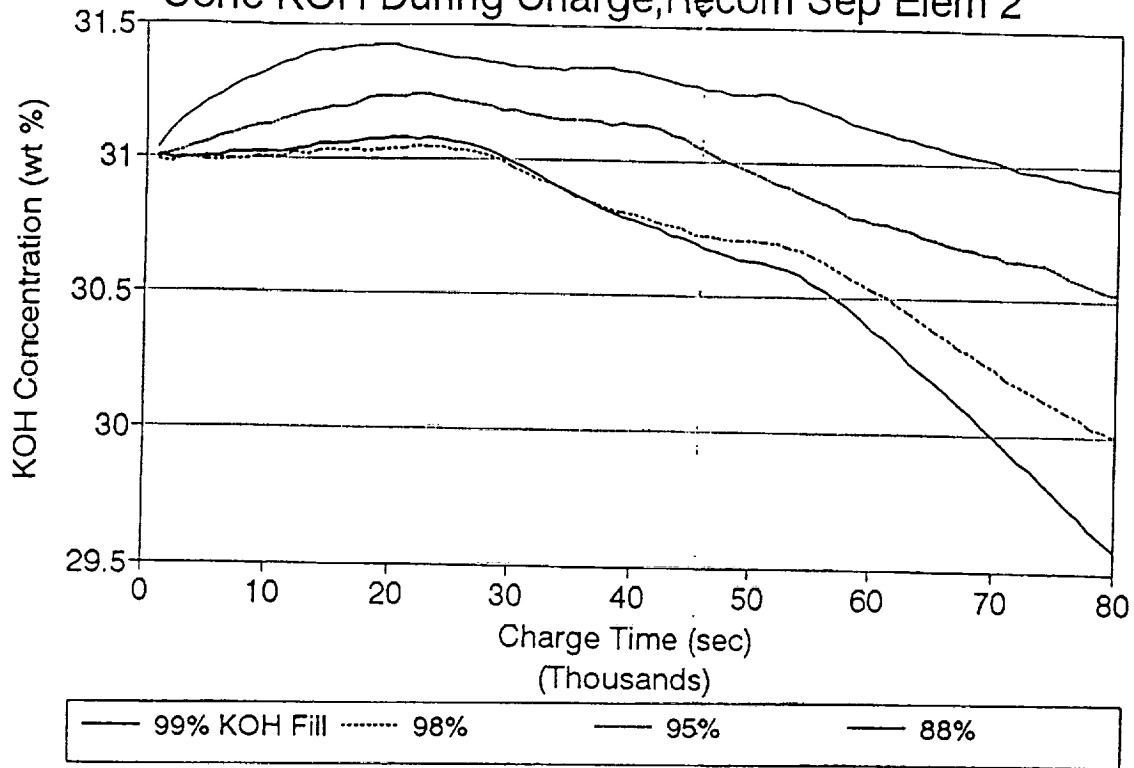


Fig. 17. Recirculating Stack NiH2 Cell  
 Conc KOH During Chg, Nickel Elem 15

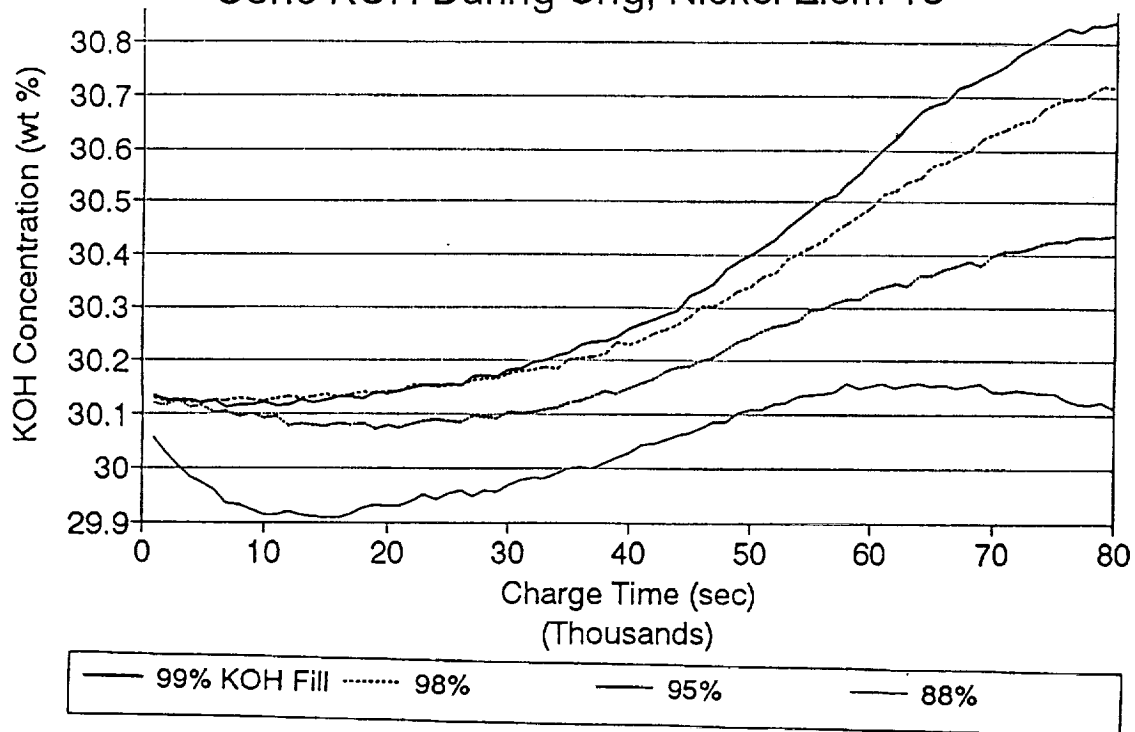


Fig. 18. Recirculating Stack NiH2 Cell  
 Conc KOH During Chg, Separator Elem 24

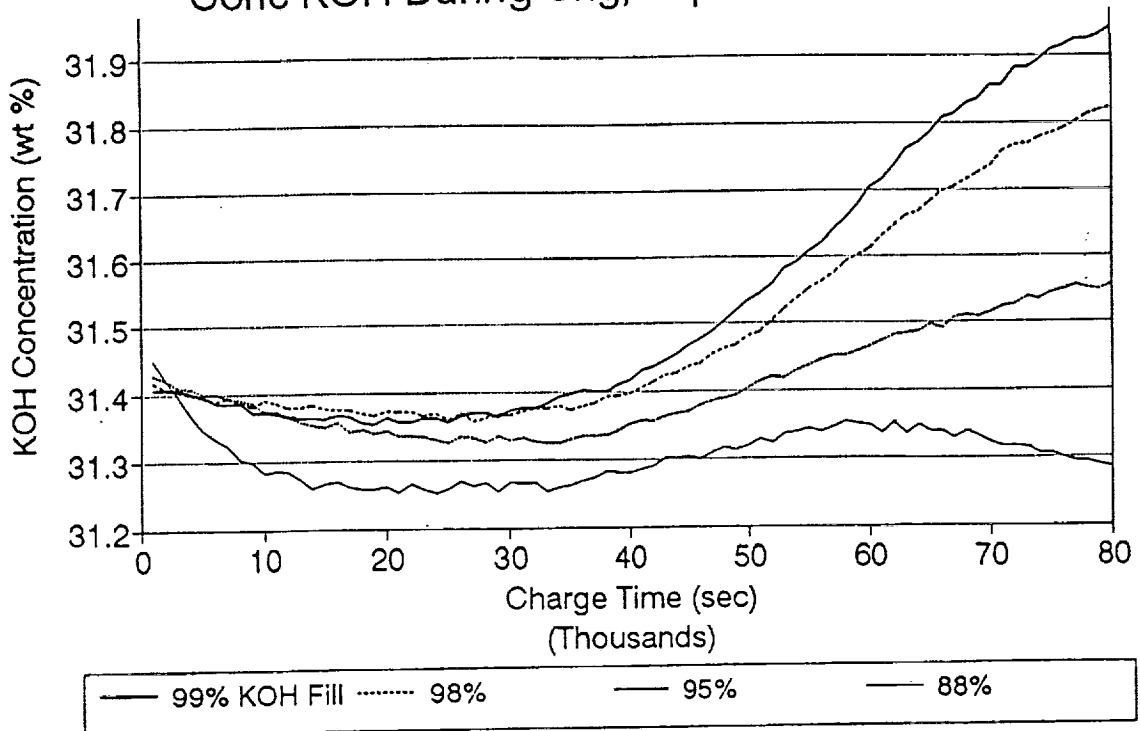


Fig. 19. Recirculating Stack NiH2 Cell  
 Conc KOH During Charge, Pt/H2 Elem 34

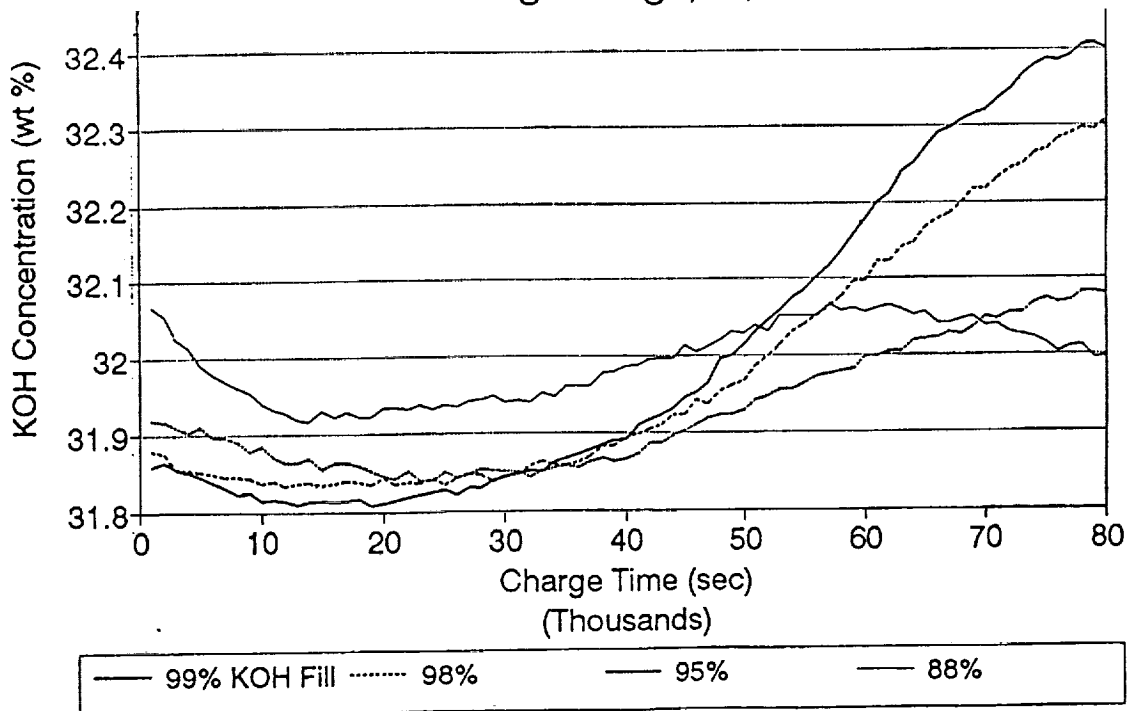


Fig. 20. Recirculating Stack NiH<sub>2</sub> Cell  
SOC in Ni Electrode at 10 Ks into Chg

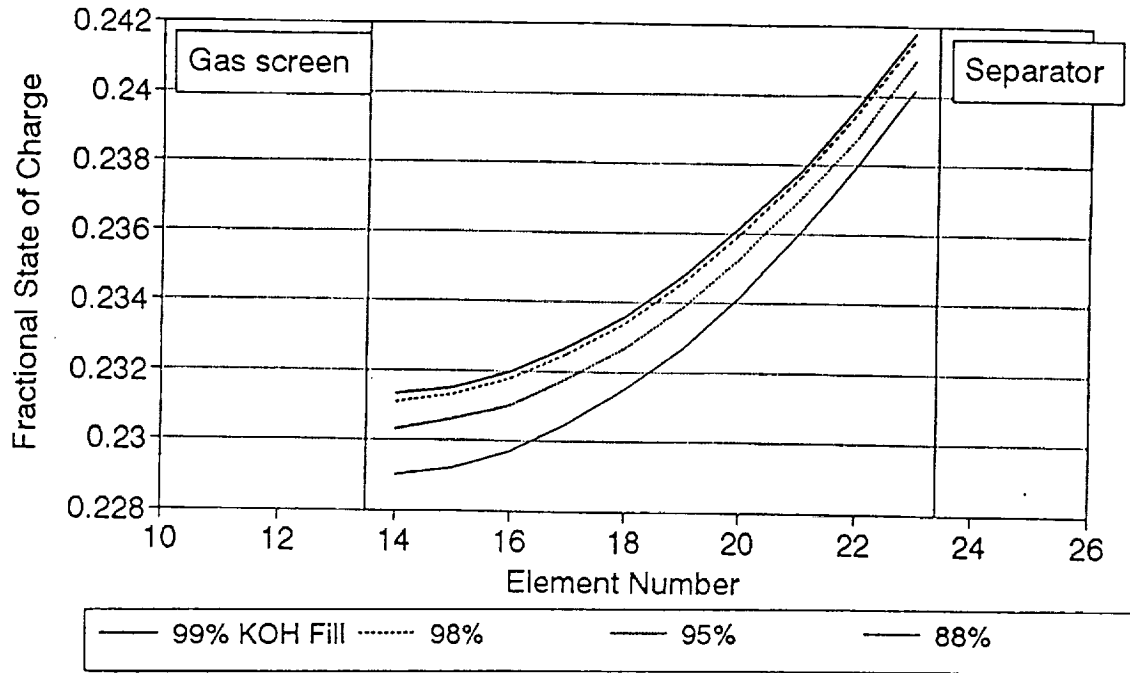


Fig. 21. Recirculating Stack NiH<sub>2</sub> Cell  
SOC in Ni Electrode at 80 Ks into Chg

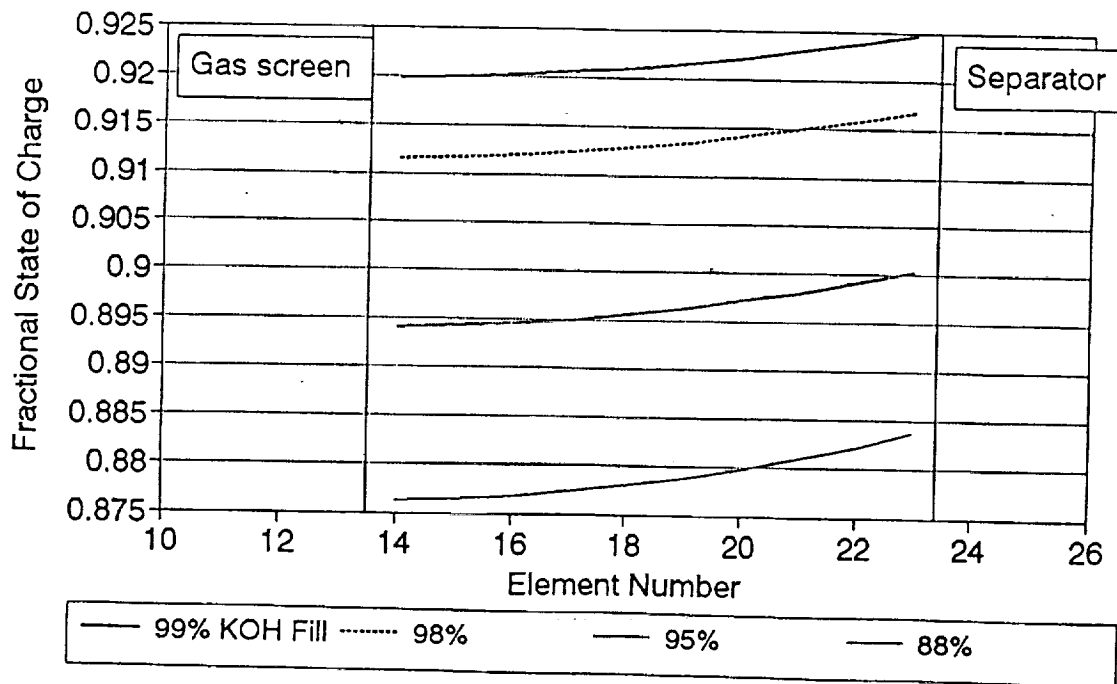


Fig. 22. Recirculating Stack NiH<sub>2</sub> Cell  
O<sub>2</sub> Pressure 80Ks into Charge, Flooded GS

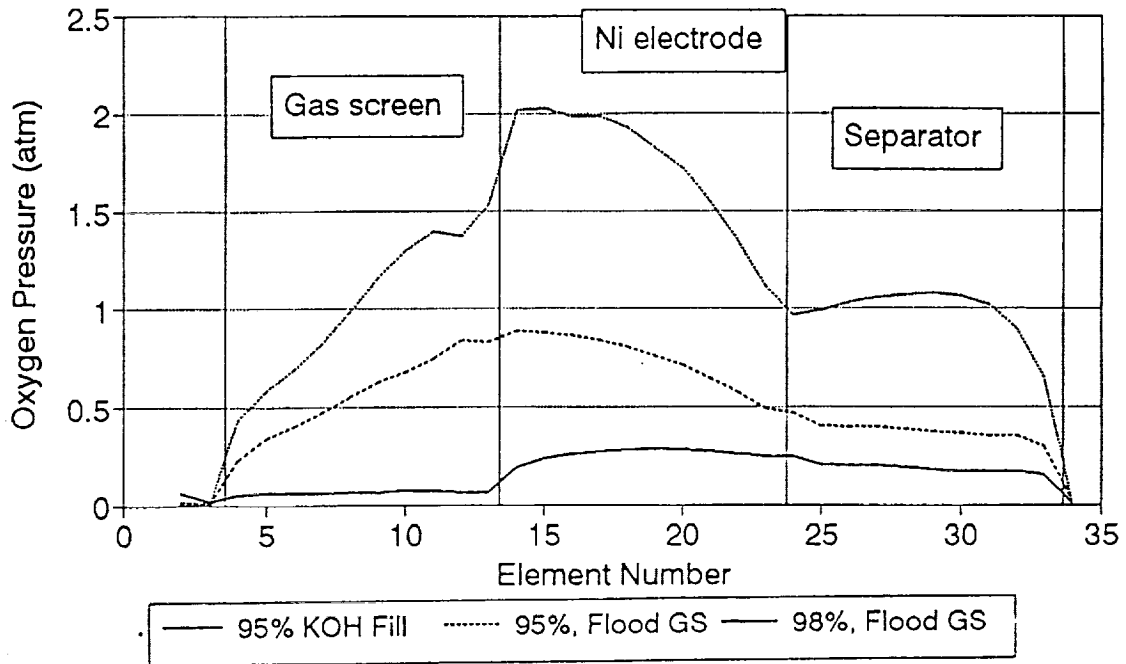


Fig. 23. Recirculating Stack NiH<sub>2</sub> Cell  
Stack Porosity 80Ks in Chg, Flooded GS

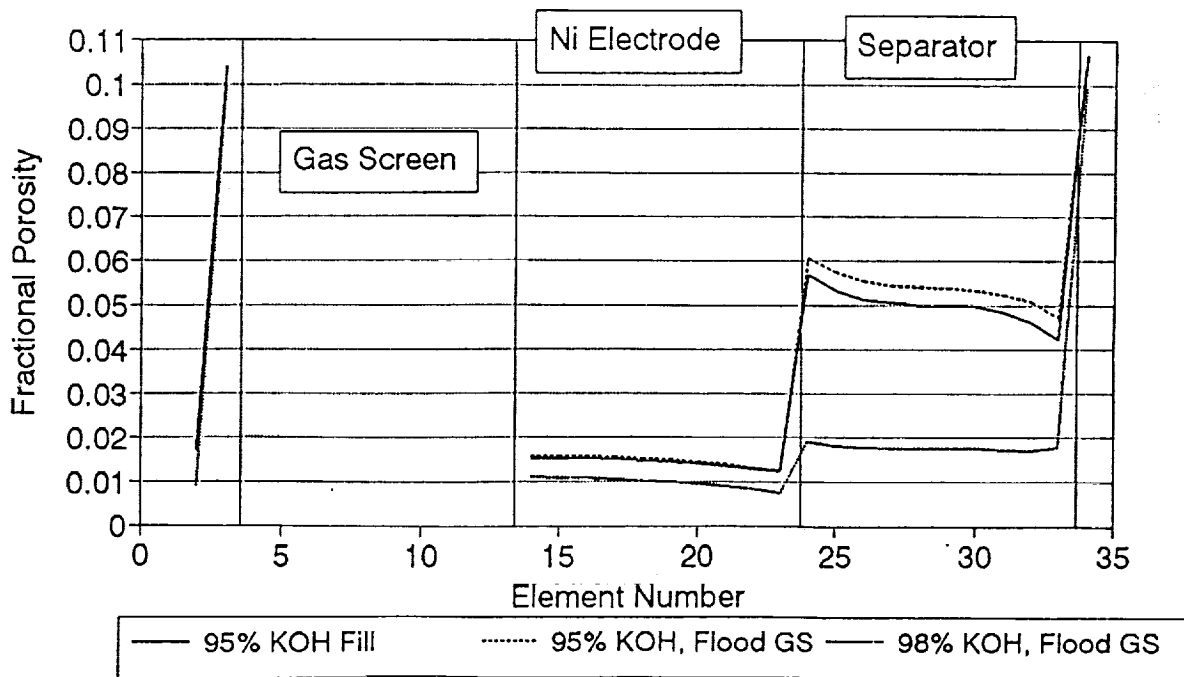


Fig. 24. Recirculating Stack NiH<sub>2</sub> Cell  
 % KOH Conc. 80Ks in Charge, Flooded GS

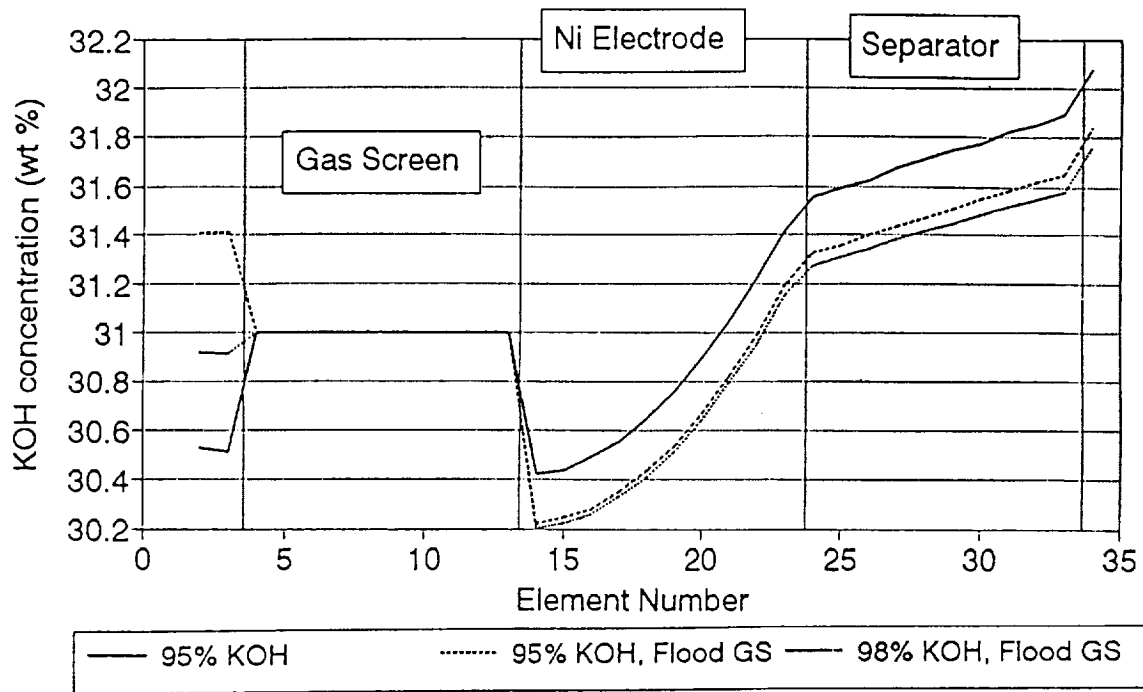


Fig. 25. Max Delta-P Across Stack  
 In recirc stack NiH<sub>2</sub> cell, 80000 s chg

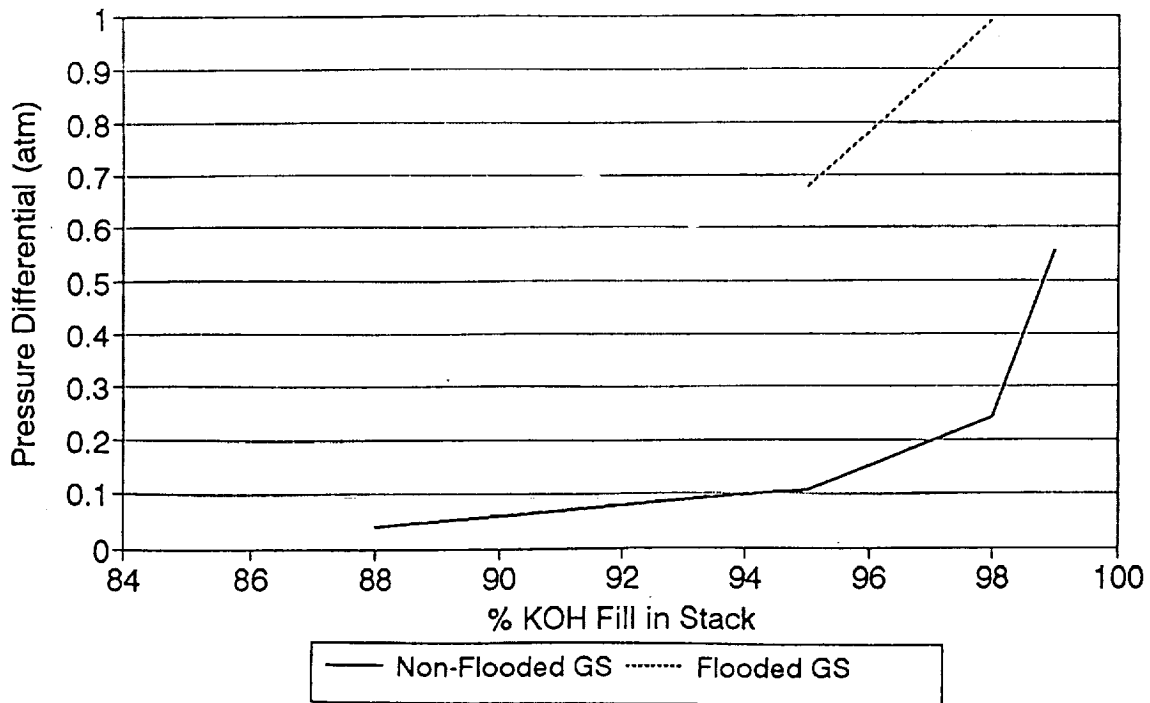


Fig. 26. Loading Profiles for Ni Electrodes  
With Various Levels of Surface Loading

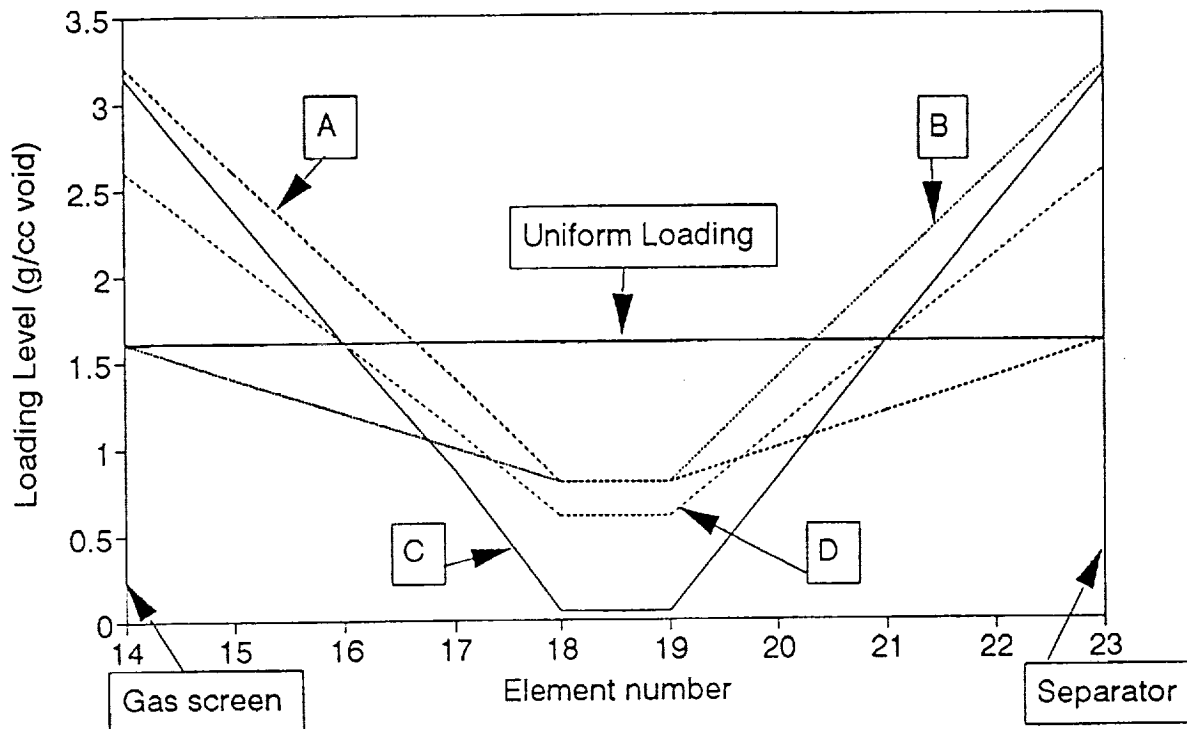


Fig 27. Oxygen Pressure Profile Through  
Stack, 80,000 sec into recharge

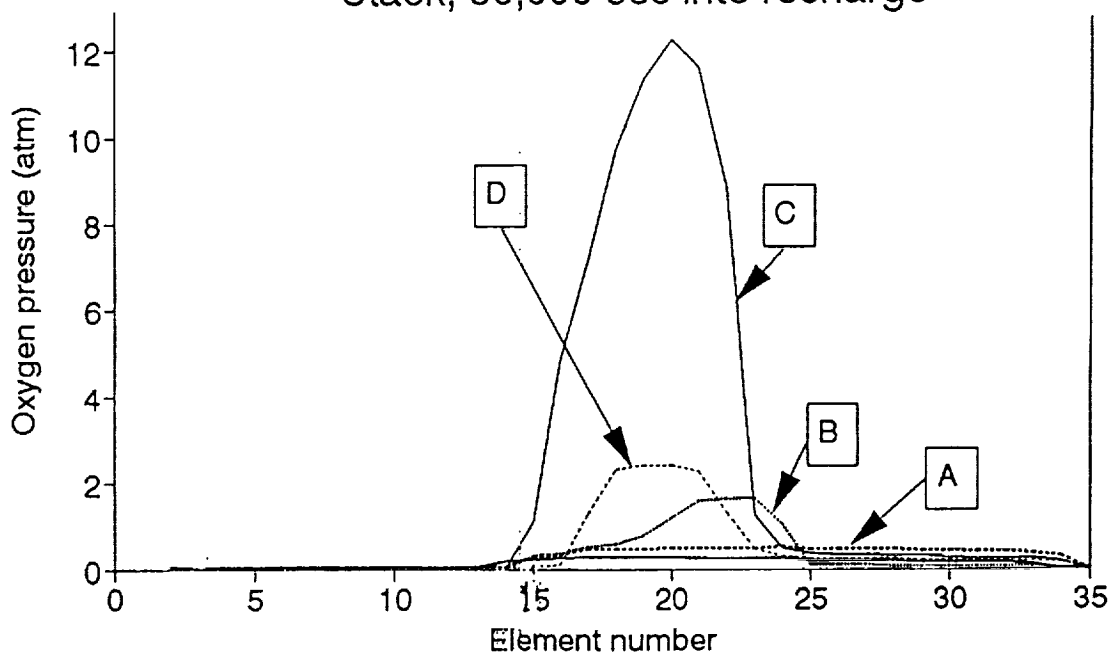


Fig 28. Total Pressure Profile Through Stack, 80,000 sec into recharge

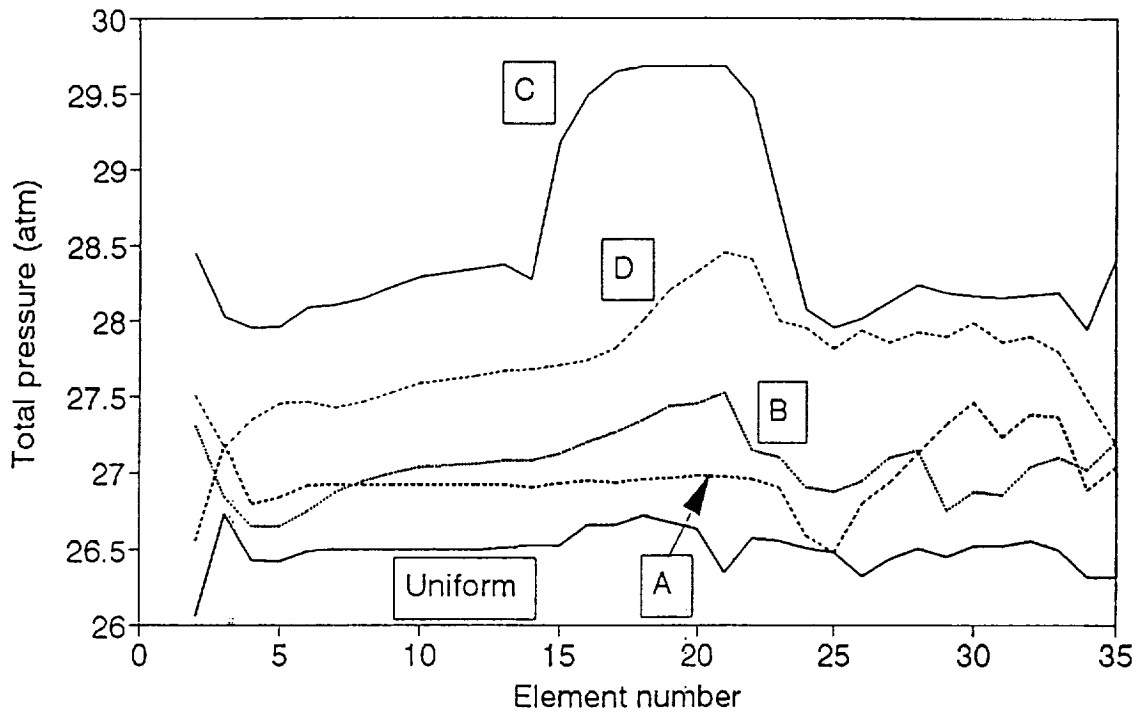


Fig 29. KOH Concentration Profile Through Stack, 80,000 sec into recharge

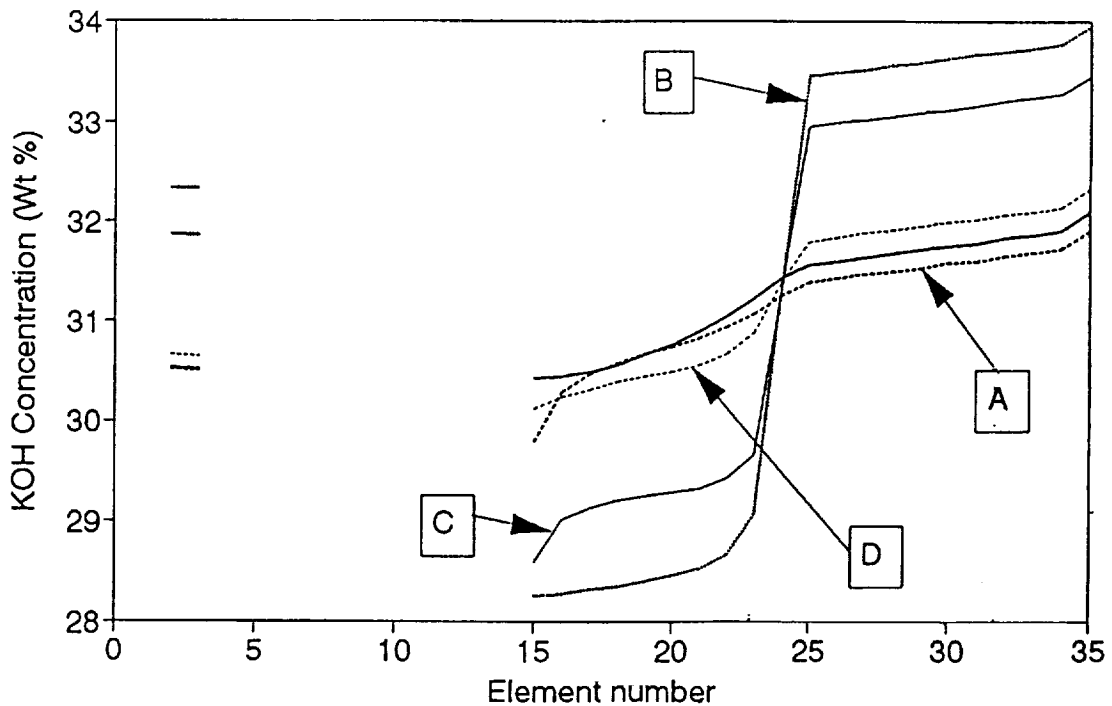


Figure 30. Oxygen Concentration  
in Recirculating Stack NiH<sub>2</sub> Cell During Overcharge,  
Uniform Loading @ 1.6 g/cc, 95% KOH Fill

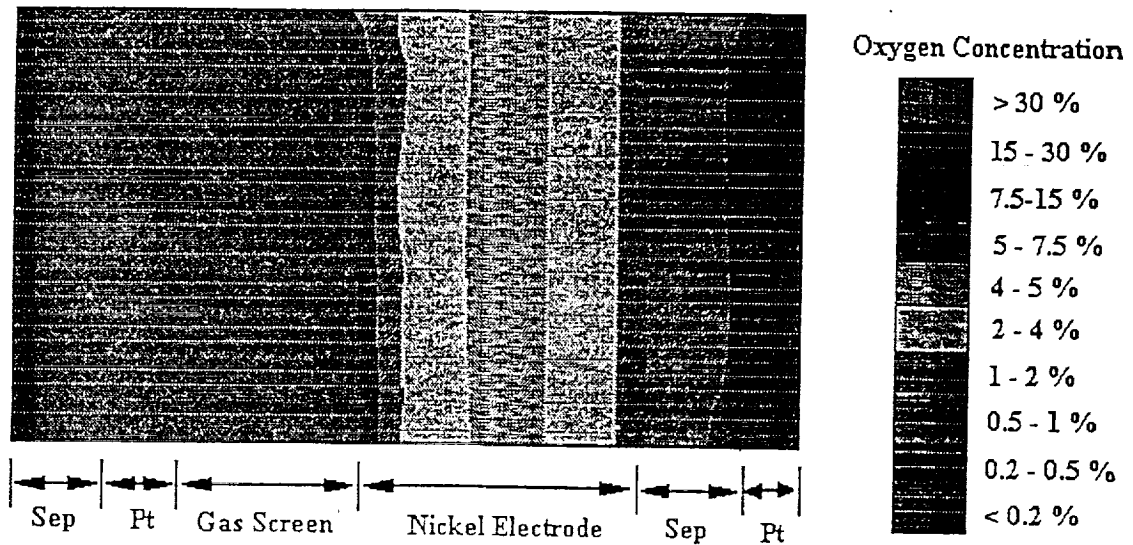


Figure 31. Oxygen Concentration Through a  
Recirculating Stack NiH<sub>2</sub> Cell with surface loading  
(3.1 g/cc void) in Overcharge

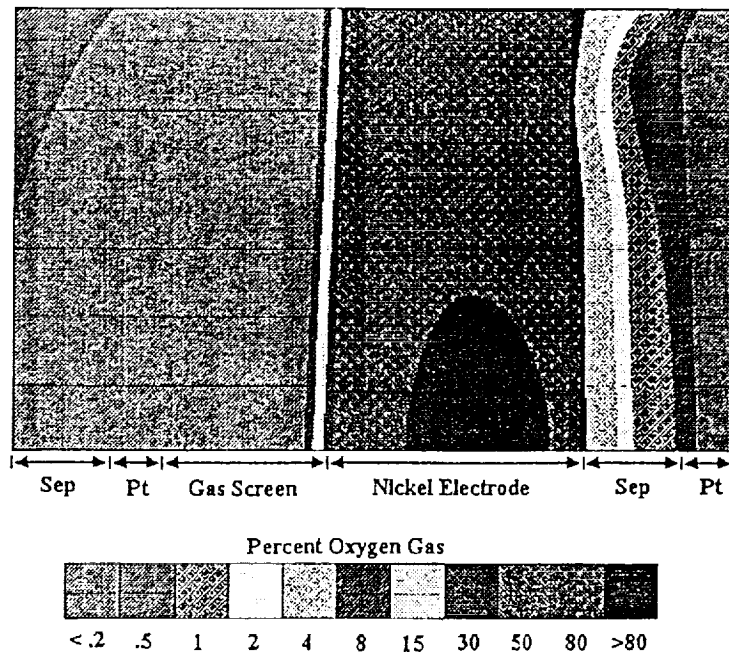


Figure 32. Oxygen Concentration in Recirculating Stack NiH<sub>2</sub> Cell with Surface Loading (3.1 g/ccv), and with surface crack on Gas screen side of Ni electrode

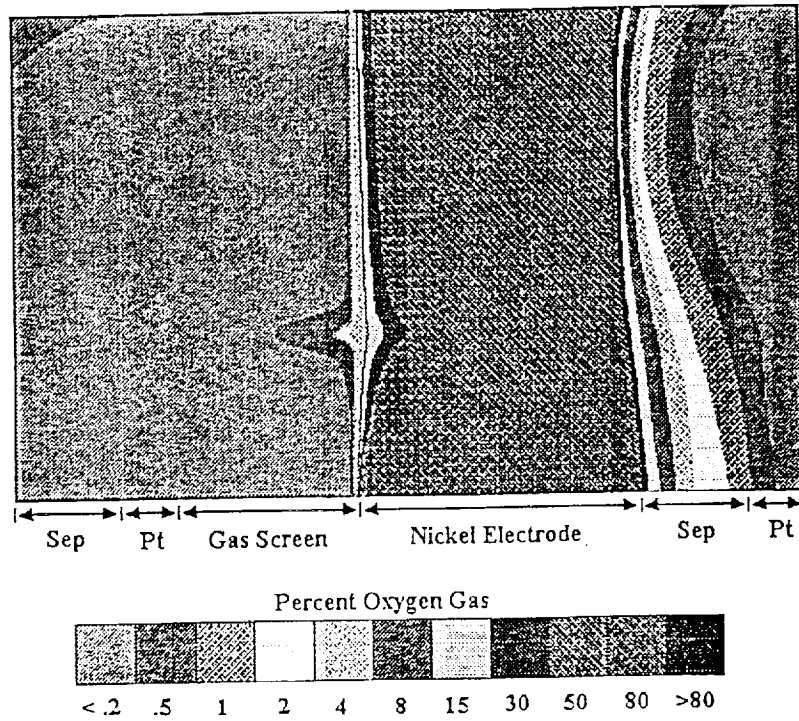
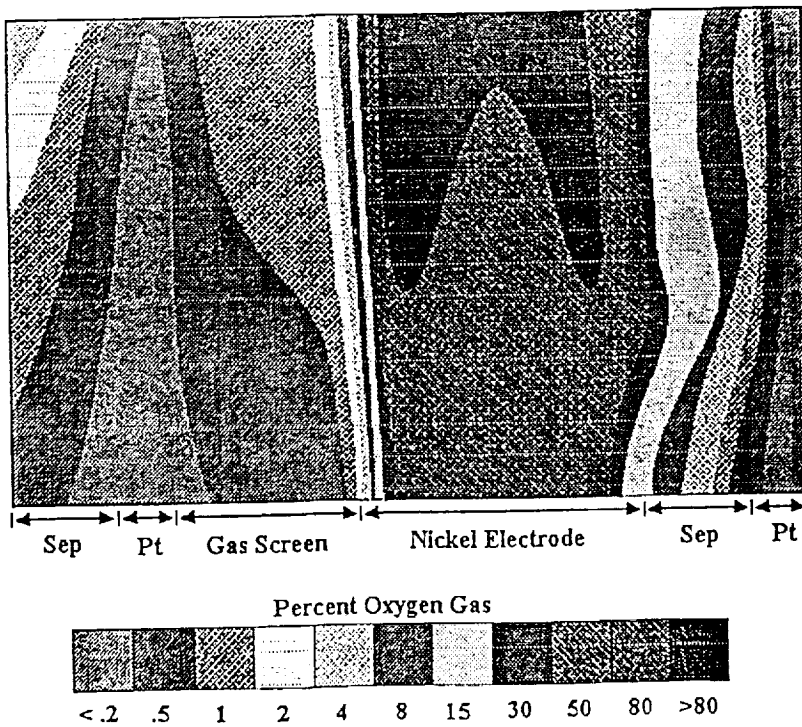


Figure 33. Oxygen Concentration in Recirculating Stack NiH<sub>2</sub> Cell with Surface Loading (3.1 g/ccv), and with surface crack on Separator side of Ni electrode.



**APPENDIX A**  
**FILE FOR NICKEL HYDROGEN CELL MODEL --**  
**RECIRCULATING STACK WITH WALL WICKS**

Number of elements is 36 KOH diffusion coeff(xE+5)is 2.13  
 Number of interfaces is 55 Temperature (deg C) is 20.00  
 Number of circuit components is 52 Ni Loading level (g/ccv) is 1.60  
 Number of Electrochemical rxns is 3 Initial KOH percentage is 31.00  
 Ni electrode plaque porosity is 0.800 Initial Nickel KOH fill is 0.950  
 Separator solid porosity is 0.500 Initial separator KOH is 0.950  
 Pt electrode porosity is 0.500 Initial Platinum KOH fill 0.950  
 Wall wick porosity is 0.500 Initial Wall wick KOH is 0.950  
 Gas screen porosity is 0.900 Ni flat band potential is -0.300  
 Ni electrode tortuosity is 2.00 Shottky I/V slope 10.000  
 Separator tortuosity is 1.20 Hydrogen diffusion coeff 7.800  
 Platinum electrode tortuosity 1.60 Total initial pressure(atm) 2.000  
 Wall wick tortuosity is 1.20 Initial beta-Ni SOC is 0.050

Electrochemical Reversible Charge Discharge Charge Discharge  
 Reaction Potential Rate const Rate const Tafel Tafel  
 Nickel-beta 1 0.490 0.1200 0.0020 77.00 77.00  
 Oxygen 2 0.400 0.1220 0.1220 52.00 52.00  
 Hydrogen 3 -0.827 0.0625 0.0625 78.00 78.00

Element Number	Type	Center Position (mm)			mm Center to Edge		
		X	Y	Z	X	Y	Z
1	5	1.0300	10.0500	0.0	1.03	0.05	5.0
2	2	0.1500	5.0000	0.0	0.15	5.0	5.0000
3	3	0.3800	5.0000	0.0	0.08	5.0	5.0000
4	4	0.4850	5.0000	0.0	0.025	5.0	5.0000
5	4	0.5350	5.0000	0.0	0.025	5.0	5.0000
6	4	0.5850	5.0000	0.0	0.025	5.0	5.0000
7	4	0.6350	5.0000	0.0	0.025	5.0	5.0000
8	4	0.6850	5.0000	0.0	0.025	5.0	5.0000
9	4	0.7350	5.0	0.0	0.025	5.0	5.0
10	4	0.785	5.0	0.0	0.025	5.0	5.0
11	4	0.835	5.0	0.0	0.025	5.0	5.0
12	4	0.885	5.0	0.0	0.025	5.0	5.0
13	4	0.935	5.0	0.0	0.025	5.0	5.0
14	1	1.000	5.0	0.0	0.04	5.0	5.0
15	1	1.08	5.0	0.0	0.04	5.0	5.0

16	1	1.16	5.0	0.0	0.04	5.0	5.0
17	1	1.24	5.0	0.0	0.04	5.0	5.0
18	1	1.32	5.0	0.0	0.04	5.0	5.0
19	1	1.40	5.0	0.0	0.04	5.0	5.0
20	1	1.48	5.0	0.0	0.04	5.0	5.0
21	1	1.56	5.0	0.0	0.04	5.0	5.0
22	1	1.64	5.0	0.0	0.04	5.0	5.0
23	1	1.72	5.0	0.0	0.04	5.0	5.0
24	2	1.775	5.0	0.0	0.015	5.0	5.0
25	2	1.805	5.0	0.0	0.015	5.0	5.0
26	2	1.835	5.0	0.0	0.015	5.0	5.0
27	2	1.865	5.0	0.0	0.015	5.0	5.0
28	2	1.895	5.0	0.0	0.015	5.0	5.0
29	2	1.925	5.0	0.0	0.015	5.0	5.0
30	2	1.955	5.0	0.0	0.015	5.0	5.0
31	2	1.985	5.0	0.0	0.015	5.0	5.0
32	2	2.015	5.0	0.0	0.015	5.0	5.0
33	2	2.045	5.0	0.0	0.015	5.0	5.0
34	3	2.140	5.0	0.0	0.08	5.0	5.0
35	0	4.220	5.0	0.0	2.00	5.0	5.0
36	0	3.340	-0.1	0.0	2.88	0.1	5.0

Interface Number	Interface Type	Element on A Side		Element on B side		Second Loop	Third Loop
		Element	Element	Element	Element		
1	2	1	2	-36	0	0	0
2	2	2	3	-36	0	0	0
3	1	3	4	-36	0	0	0
4	0	4	5	-36	-46	0	0
5	0	5	6	-36	0	-47	0
6	0	6	7	-36	-48	0	0
7	0	7	8	-36	0	-49	0
8	0	8	9	-36	-50	0	0
9	0	9	10	-36	0	-51	0
10	0	10	11	-36	-52	0	0
11	0	11	12	-36	0	-53	0
12	0	12	13	-36	-54	0	0
13	1	13	14	-36	0	-55	0
14	2	14	15	-36	0	-55	0
15	2	15	16	-36	0	-55	0
16	2	16	17	-36	0	-55	0

Entry component interface area is 0.00800 cm<sup>2</sup>, and distance is 0.50000 cm  
 Exit component interface area is 0.01200 cm<sup>2</sup>, and distance is 0.50000 cm  
 Component Component Inter A-side B-Side A-Side B-Side A-Side B-Side Loop Eqs

Number	Type	Face	Elem	Elem	Node	Node	A	B	C	D
1	7	22	22	23	2	1	0	51	0	0
2	7	21	22	22	3	2	0	49	0	0
3	7	20	20	21	4	3	0	47	0	0
4	7	19	19	20	5	4	0	45	0	0
5	7	18	18	19	7	5	0	43	0	0
6	7	0	0	19	6	5	0	0	0	0
7	7	17	17	18	8	7	0	41	0	0
8	7	16	16	17	9	8	0	39	0	0
9	7	15	15	16	10	9	0	37	0	0
10	7	14	14	15	11	10	0	35	0	0
11	1	-1	14	14	11	12	-34	0	0	0
12	2	14	14	15	12	13	0	-35	0	0
13	2	15	15	16	13	14	0	-37	0	0
14	2	16	16	17	14	15	0	-39	0	0
15	2	17	17	18	15	16	0	-41	0	0
16	2	18	18	19	16	17	0	-43	0	0
17	2	19	19	20	17	18	0	-45	0	0
18	2	20	20	21	18	19	0	-47	0	0
19	2	21	21	22	19	20	0	-49	0	0
20	2	22	22	23	20	21	0	-51	0	0
21	2	23	23	24	21	22	0	0	0	0
22	2	24	24	25	22	23	0	0	0	0
23	2	25	25	26	23	24	0	0	0	0
24	2	26	26	27	24	25	0	0	0	0
25	2	27	27	28	25	26	0	0	0	0
26	2	28	28	29	26	27	0	0	0	0
27	2	29	29	30	27	28	0	0	0	0
28	2	30	30	31	28	29	0	0	0	0
29	2	31	31	32	29	30	0	0	0	0
30	2	32	32	33	30	31	0	0	0	0
31	2	33	33	34	31	32	0	0	0	0
32	3	-1	34	34	32	33	0	0	0	0
33	7	0	34	0	33	34	0	0	0	0
34	4	-1	14	14	11	12	34	-35	0	0
35	1	-1	15	15	10	13	-36	35	0	0
36	4	-1	15	15	10	13	36	-37	0	0
17	2	17	17	18	17	18	0	-55	0	-55
18	2	18	18	19	18	19	0	-55	0	-55
19	2	19	19	20	19	20	0	-55	0	-55
20	2	20	20	21	20	21	0	-55	0	-55
21	2	21	21	22	21	22	0	-55	0	-55
22	2	22	22	23	22	23	0	-55	0	-55
23	2	23	23	24	23	24	0	-55	0	-55
24	2	24	24	25	24	25	0	-37	-55	0
25	2	25	25	26	25	26	0	-38	0	-55
26	2	26	26	27	26	27	0	-39	0	-55
27	2	27	27	28	27	28	0	-40	0	-55
28	2	28	28	29	28	29	0	-41	0	-55
29	2	29	29	30	29	30	0	-42	0	-55
30	2	30	30	31	30	31	0	-43	0	-55
31	2	31	31	32	31	32	0	-44	0	-55
32	2	32	32	33	32	33	0	-45	0	-55
33	2	33	33	34	33	34	0	0	0	-55
34	1	34	34	35	34	35	0	0	0	-55
35	0	35	35	36	35	36	0	0	0	-55
36	2	1	36	36	36	37	0	-37	0	-55
37	2	1	37	37	37	38	0	-38	0	-55
38	2	1	38	38	38	39	0	-39	0	-55
39	2	1	39	39	39	40	0	-40	0	-55
40	2	1	40	40	40	41	0	-41	0	-55
41	2	1	41	41	41	42	0	-42	0	-55
42	2	1	42	42	42	43	0	-43	0	-55
43	2	1	43	43	43	44	0	-44	0	-55
44	2	1	44	44	44	45	0	-45	0	-55
45	2	1	45	45	45	46	0	-46	0	-55
46	0	4	46	46	46	47	0	-47	0	-55
47	0	5	47	47	47	48	0	-48	0	-55
48	0	6	48	48	48	49	0	-49	0	-55
49	0	7	49	49	49	50	0	-50	0	-55
50	0	8	50	50	50	51	0	-51	0	-55
51	0	9	51	51	51	52	0	-52	0	-55
52	0	10	52	52	52	53	0	-53	0	-55
53	0	11	53	53	53	54	0	-54	0	-55
54	0	12	54	54	54	55	0	-55	0	-55
55	0	13	55	55	55	56	0	-56	0	-55

37 1 -1 16 16 9 14 -38 37 0 0  
 38 4 -1 16 16 9 14 38 -39 0 0  
 39 1 -1 17 17 8 15 -40 39 0 0  
 40 4 -1 17 17 8 15 40 -41 0 0  
 41 1 -1 18 18 7 16 -42 41 0 0  
 42 4 -1 18 18 7 16 42 -43 0 0  
 43 1 -1 19 19 5 17 -44 43 0 0  
 44 4 -1 19 19 5 17 44 -45 0 0  
 45 1 -1 20 20 4 18 -46 45 0 0  
 46 4 -1 20 20 4 18 46 -47 0 0  
 47 1 -1 21 21 3 19 -48 47 0 0  
 48 4 -1 21 21 3 19 48 -49 0 0  
 49 1 -1 22 22 2 20 -50 49 0 0  
 50 4 -1 22 22 2 20 50 -51 0 0  
 51 1 -1 23 23 1 21 -52 51 0 0  
 52 4 -1 23 23 1 21 52 0 0

The following program contains 1 steps

Program Step Current Time(sec)/ Save Time Calculation  
 Step Type (ma) V-Limit Interval Time Interval  
 1 1 2.0000 80000.0 1000.0 2.000

**APPENDIX B.**  
 2 D NI<sub>2</sub> CELL MODEL W/SURFACE CRACK,  
 RECIRCULATING STACK WITH WALL WICKS

Number of elements is 45 KOH diffusion coeff(xE+5)is 2.13  
 Number of interfaces is 83 Temperature (deg C) is 20.00  
 Number of circuit components is 95 Ni Loading level (g/ccv) is 1.60  
 Number of Electrochemical rxns is 3 Initial KOH percentage is 31.00  
 Ni electrode plaque porosity is 0.800 Initial Nickel KOH fill is 0.950  
 Separator solid porosity is 0.500 Initial separator KOH is 0.950  
 Pt electrode porosity is 0.500 Initial Platinum KOH fill 0.950  
 Wall wick porosity is 0.500 Initial Wall wick KOH is 0.950  
 Gas screen porosity is 0.900 Ni flat band potential is -0.300  
 Ni electrode tortuosity is 2.00 Shottky I/V slope 10.000  
 Separator tortuosity is 1.20 Hydrogen diffusion coeff 7.800  
 Platinum electrode tortuosity 1.60 Total initial pressure(atm) 25.000  
 Wall wick tortuosity is 1.20 Initial beta-Ni SOC is 0.900

Electrochemical Reaction	Reversible Potential	Charge Rate const	Discharge Rate const	Charge Tafel	Discharge Tafel
Nickel-beta 1	0.490	0.1200	0.0020	77.00	77.00
Oxygen 2	0.400	0.1220	0.1220	52.00	52.00
Hydrogen 3	-0.827	0.0625	0.0625	78.00	78.00

Element Number	Element Type	Center Position (mm) X	Center Position (mm) Y	Center Position (mm) Z	mm Center to Edge X	mm Center to Edge Y	mm Center to Edge Z
1	3	0.380	5.0	0.0	0.08	5.0	5.0
2	2	0.1500	5.0000	0.0	0.15	5.0	5.0000
3	5	1.0350	10.0500	0.0	1.035	0.05	5.0
4	2	2.0200	8.3500	0.0	0.05	1.65	5.0000
5	2	1.9200	8.3500	0.0	0.05	1.65	5.0000
6	2	1.8200	8.3500	0.0	0.05	1.65	5.0000
7	1	1.6700	8.3500	0.0	0.100	1.65	5.0000
8	1	1.3700	8.3500	0.0	0.200	1.65	5.0000
9	1	1.0700	8.3500	0.0	0.100	1.65	5.0000
10	4	0.8850	8.35	0.0	0.085	1.65	5.0
11	4	0.715	8.35	0.0	0.085	1.65	5.0
12	4	0.545	8.35	0.0	0.085	1.65	5.0
13	4	0.545	5.05	0.0	0.085	1.65	5.0
14	4	0.715	5.05	0.0	0.085	1.65	5.0
15	4	0.885	5.05	0.0	0.085	1.65	5.0
16	1	1.070	5.05	0.0	0.100	1.65	5.0
17	1	1.370	5.05	0.0	0.200	1.65	5.0
18	1	1.670	5.05	0.0	0.100	1.65	5.0
19	2	1.820	5.05	0.0	0.05	1.65	5.0
20	2	1.920	5.05	0.0	0.05	1.65	5.0
21	2	2.020	5.05	0.0	0.05	1.65	5.0
22	2	2.020	3.35	0.0	0.05	0.05	5.0
23	2	1.920	3.35	0.0	0.05	0.05	5.0
24	2	1.820	3.35	0.0	0.05	0.05	5.0
25	1	1.670	3.35	0.0	0.100	0.05	5.0
26	1	1.370	3.35	0.0	0.200	0.05	5.0
27	1	1.070	3.35	0.0	0.100	0.05	5.0
28	4	0.885	3.35	0.0	0.085	0.05	5.0
29	4	0.715	3.35	0.0	0.085	0.05	5.0
30	4	0.545	3.35	0.0	0.085	0.05	5.0
31	4	0.545	1.65	0.0	0.085	1.65	5.0
32	4	0.715	1.65	0.0	0.085	1.65	5.0



65	2	17	26	-64	65	0	15	2	64	16	27	16	15	76	47	0	0
66	2	18	25	66	-65	0	16	2	54	9	16	17	16	48	0	75	0
67	2	19	24	-66	67	0	17	2	8	9	8	17	18	0	-49	-75	0
68	2	20	23	68	-67	0	18	2	55	8	17	18	19	0	-78	-75	0
69	0	29	32	0	-70	69	19	2	65	17	26	19	20	-76	56	-79	0
70	0	28	33	-71	70	0	20	2	72	26	35	20	21	0	-77	55	-80
71	2	27	34	71	-72	0	21	2	35	35	36	21	22	54	0	0	-80
72	2	26	35	-73	72	0	22	2	73	25	36	23	22	83	-53	0	80
73	2	25	36	73	-74	0	23	2	66	18	25	24	23	-52	82	79	0
74	2	24	37	-75	74	0	24	2	56	7	18	25	24	81	78	-51	0
75	2	23	38	75	-76	0	25	2	6	7	6	25	26	-81	0	0	0
76	2	22	39	-77	76	0	26	2	57	6	19	26	27	-81	-84	0	0
77	2	22	41	77	-78	0	27	2	67	19	24	27	28	-85	-82	0	0
78	2	21	42	0	78	-60	28	2	74	24	37	28	29	-83	-86	0	0
79	1	42	44	-80	79	0	29	2	37	37	38	29	30	0	-86	0	0
80	1	41	44	80	-81	0	30	2	75	23	38	31	30	89	86	0	0
81	1	40	44	0	81	-82	31	2	68	20	23	32	31	85	88	0	0
82	0	33	45	-83	0	82	32	2	58	5	20	33	32	87	84	0	0
83	0	32	45	83	-45	0	33	2	4	5	4	33	34	-87	0	0	0
							34	2	59	4	21	34	35	-87	-90	0	0
							35	2	21	21	22	35	36	-91	-88	0	0
							36	2	76	22	39	36	37	-89	-92	0	0
							37	2	39	39	40	37	38	0	-92	0	0
							38	2	40	41	40	39	38	95	92	0	0
							39	2	41	42	41	40	39	91	-94	0	0
							40	2	42	43	42	41	40	93	90	0	0
							41	3	-1	43	43	41	42	-93	0	0	0
							42	7	42	43	42	42	43	-93	0	0	0
							43	7	41	42	41	43	44	0	-94	0	0
							44	7	40	41	40	44	45	-95	0	0	0
							45	7	0	40	0	45	46	0	0	0	0
							46	1	-1	27	27	8	15	46	-47	-58	0
							47	1	-1	16	16	7	16	-48	47	-59	0
							48	1	-1	9	9	2	17	48	-49	-60	0
							49	1	-1	8	8	3	18	-50	49	-61	0
							50	1	-1	7	7	4	25	50	-62	-51	0
							51	1	-1	18	18	5	24	-52	-63	51	0
							52	1	-1	25	25	10	23	52	-53	-64	0
							53	1	-1	36	36	11	22	-54	53	-65	0
							54	1	-1	35	35	12	21	54	-66	-55	0

Entry component interface area is 0.04000 cm<sup>2</sup>, and distance is 0.12500 cm

Exit component interface area is 0.01600 cm<sup>2</sup>, and distance is 0.12500 cm

Component Component Inter A-side B-Side A-Side B-Side Loop

Equations Number	Type	Face	Elem	Elem	Node	Node	A	B	C	D
1	7	0	9	1	2	0	0	0	0	
2	7	8	9	8	2	3	0	49	-69	0
3	7	7	8	7	3	4	50	-70	0	0
4	7	56	7	18	4	5	0	-70	51	0
5	7	17	17	18	6	5	0	70	72	0
6	7	16	16	17	7	6	71	0	69	0
7	7	64	16	27	7	8	-71	-47	0	0
8	7	26	27	26	8	9	-71	-73	0	0
9	7	25	26	25	9	10	0	0	-72	-74
10	7	73	25	36	10	11	0	53	0	-74
11	7	35	35	36	12	11	-54	0	0	74
12	7	34	34	35	13	12	0	73	0	0
13	1	-1	34	34	13	14	-46	-57	0	0
14	2	71	27	34	15	14	46	77	0	0

94	3	-1	41	41	39	44	-95	94	0	0
95	3	-1	40	40	38	45	95	0	0	0

The following program contains 1 steps

Program	Step	Current	Time(sec)/	Save	Time	Calculation
Step	Type	(ma)	V-Limit	Interval	Interval	Time Interval
1	1	2.0000	80000.0	1000.0	2.000	

55	1	-1	26	9	20	-67	-56	55	0
56	1	-1	17	6	19	-68	56	0	0
57	4	-1	34	13	14	0	57	0	0
58	4	-1	27	8	15	0	0	58	0
59	4	-1	16	7	16	0	0	59	0
60	4	-1	9	2	17	0	0	60	0
61	4	-1	8	3	18	0	0	61	0
62	4	-1	7	4	25	0	62	0	0
63	4	-1	18	5	24	0	63	0	0
64	4	-1	25	10	23	0	0	64	0
65	4	-1	36	11	22	0	0	65	0
66	4	-1	35	12	21	0	66	0	0
67	4	-1	26	9	20	67	0	0	0
68	4	-1	17	6	19	68	0	0	0
69	7	54	9	2	7	-48	0	69	0
70	7	55	8	3	6	0	70	-69	0
71	7	65	17	6	9	71	-56	-72	0
72	7	66	18	5	10	52	0	72	0
73	7	71	27	8	13	-46	73	0	0
74	7	72	26	9	12	0	-73	-55	74
75	2	16	16	16	19	-76	0	75	0
76	2	26	27	15	20	76	-77	0	0
77	2	34	34	14	21	0	77	0	0
78	2	7	7	18	25	-50	78	0	0
79	2	17	17	19	24	0	-78	79	0
80	2	25	26	20	23	0	0	-79	80
81	2	18	18	24	27	81	-82	0	0
82	2	24	25	23	28	-83	82	0	0
83	2	36	36	22	29	83	0	0	0
84	2	5	6	26	33	0	84	0	0
85	2	19	19	20	32	85	-84	0	0
86	2	23	24	28	31	-85	86	0	0
87	2	20	20	32	35	87	-88	0	0
88	2	22	23	31	36	-89	88	0	0
89	2	38	38	30	37	89	0	0	0
90	2	60	4	43	41	0	90	0	0
91	2	78	21	42	40	91	-90	0	0
92	2	77	22	41	39	-91	92	0	0
93	3	-1	42	42	43	93	-94	0	0

